This is a preprint, the final version is subject to change, of the American Mineralogist (MSA)
Cite as Authors (Year) Title. American Mineralogist, in press.
(DOI will not work until issue is live.) DOI: http://dx.doi.org/10.2138/am-2016-5357 



# Ca-Al-silicate inclusions in natural moissanite (SiC)

SIMONPIETRO DI PIERRO[1,*] AND EDWIN GNOS[2]

[1]UMR CNRS 5570, Laboratoire de Sciences de la Terre, ENS Lyon, France

[*]Present address: Applied Mineralogy Group, Saint-Gobain Recherche, Aubervilliers Cedex, F-93303, France. E-mail: simonpietro.dipierro@saint-gobain.com

[2]Natural History Museum of Geneva, route de Malagnou 1, CP 6434, 1211 Geneve 6, Switzerland

## ABSTRACT

Hundred μm-sized Calcium-Aluminum-Silicates (CAS) inclusions occur in moissanite-4H, -15R and -6H from Turkey. These inclusions commonly consist of tabular exsolution lamellae of two different minerals. By combined electron microprobe and Raman spectroscopy analysis, at least eight different, essentially Mg- and Fe-free Ca-Al-silicate or Al-silicate phases have been discerned. The most common phase is dmisteinbergite, a hexagonal modification of $CaAl_2Si_2O_8$, occurring in association with lamellae of $Ca_x(Al,Si)_{1-x}O_3$ or $Ca_{1-x}(Al,Si)_{2+x}O_5$ compositions. All three phases contain significant amounts of BaO (up to 2 mol% of celsiane component in dmisteinbergite), SrO, $SO_2$ and Light Rare Earth Elements (LREE). In particular, $Ca_{1-x}(Al,Si)_{2+x}O_5$ contains up to 2.1wt% of LREE, 3.9wt% of F and significant traces of Cl, while it is also associated to osbornite (TiN). Pure ghelenite, $Ca_2Al_2SiO_7$, and three additional compositions, namely $CaAl_{4-x}Si_xO_7$, $Ca_{1-x}(Al,Si)_{3+x}O_6$ and $Ca_{3-x}(Al,Si)_{6+x}O_{14}$ have been found, either occurring as single grains or forming exsolution lamellae. They also contain significant

amounts of BaO, SrO, $SO_2$ and LREE. One last intriguing phase is composed in average of 65.9wt % $SiO_2$, 17.4% $Al_2O_3$, 3.0% alkalis, 6.0% BaO, 2.0% CaO+MgO, 0.9% $ZrO_2$ and up to 0.5% LREE. Dmisteinbergite and ghelenite show Raman peaks in very-good agreement with literature data, $Ca_x(Al,Si)_{1-x}O_3$ shows main Raman modes at 416 and 1009 $cm^{-1}$, $Ca_{1-x}(Al,Si)_{3+x}O_6$ at 531 and 1579 $cm^{-1}$ while $Ca_{3-x}(Al,Si)_{6+x}O_{14}$ has a strong peak at 553 $cm^{-1}$. $CaAl_{4-x}Si_xO_7$ shows a weak Raman pattern, while $Ca_{1-x}(Al,Si)_{2+x}O_5$ has no detectable Raman modes. Since the association moissanite-CAS is thermodynamically not stable at ambient pressure and moissanite crystals hosting the CAS phases have $\delta^{13}C$ values typical of deep-mantle origin, we interpret the CAS inclusions as partially retrogressed HP minerals. Striking analogies exist between observed CAS compositions and experimentally-obtained HP-HT mineralogy. For instance, $Ca_x(Al,Si)_{1-x}O_3$ contains up to 25 mol% of $Al_2O_3$, which is considered as the upper limit of alumina solubility in Ca-perovskite. The study confirms that CAS phases are an important mantle depository for large ion lithophile elements (LILE) and LREE.

**Keywords:** Moissanite, dmisteinbergite, gehlenite, unknown CAS mineral, Raman spectra, mineral composition

## INTRODUCTION

The natural occurrence of moissanite, natural α-silicon carbide, under terrestrial conditions was vigorously debated until the end of the 1980s'. Milton and Vitaliano (1984) critically but correctly proposed a series of six independent criteria to discern natural moissanite occurrences from synthetic SiC contaminations. Extensive field researches in the last three decades fulfilled most of these criteria. The first one concerned the *finding of moissanite as inclusion in other*

47 *minerals*. In fact, moissanite crystals were reported included in diamonds and carbonados from
48 kimberlites and lamproites from many continental cratons in Russia (Yakutia; Marshintsev 1990),
49 China (Fuxian; Leung 1990), USA (Colorado; McCammon et al. 1997; Otter and Gurney 1986;
50 1989), South Africa (Monastery Mine; Moore et al. 1986; Moore and Gurney 1989;
51 Koffiefontein mine, Klein-BenDavid et al. 2007), Central Africa (De et al. 1998), Australia
52 (Argyle lamproite; Jacques et al. 1989), and Brazil (Sao Luis River placers; Wilding et al. 1991;
53 Svizero 1995; De et al. 1998; Kaminsky 2012). Moissanite was also reported included in garnets
54 from a Chinese retrogressive eclogite (Qi et al. 2007). These authors show excellent thin section
55 microphotographs of a dozen of moissanite crystals included, along with coesite and rutile, in
56 pyrope. In serpentinite from the Chinese Dabie Mountains, Xu et al. (2008) present thin section
57 microphotographs of moissanite associated to rutile and baddeleyite. Moreover, moissanite was
58 also reported as inclusions in olivine from the diamondiferous Karashoho pipe from the Bukantau
59 mountains from Uzbekistan (Golovko and Kaminsky 2010), and in garnets from felsic granulites
60 from the Moldanubian Zone of the Bohemian Massif (Perraki and Faryad 2014). These latter
61 authors also show thin section microphotographs where moissanite is unequivocally contained
62 within the hosting mineral. Finally, from the Luobusa ophiolite, Tibet, Robinson et al. (2015) and
63 Liang et al. (2014), reported moissanite in olivine from peridotite, and in Cr-spinel from dunite,
64 respectively. *Euhedral, unbroken crystals*, the second criterion, have been reported from Fuxian
65 (Leung et al. 1990; Leung 1990), Turkey (Di Pierro et al. 2003) and Yakutia (Shiryaev et al.
66 2011), while abundant silicon and Fe-silicides, systematically reported as inclusions in terrestrial
67 moissanite and considered to represent former *melt-inclusions* (Marschintsev 1990; Pankov and
68 Spetius 1990, Mathez et al. 1995; Bai et al. 1993; 2000; 2003; Di Pierro et al. 2003; Robinson et
69 al. 2004), is the third criterion to distinguish synthetic from natural moissanite. Besides the
70 above-mentioned Chinese findings, *freshly broken rocks showing abundant enclosed SiC*, the

fourth criterion, have been reported by Bauer et al. (1963), Leung (1988) and Di Pierro et al. (2003). The fifth criterion proposed by Milton and Vitaliano (1984) is to find *moissanite in eutectic or sutured intergrowth with magmatic minerals*. Mathez et al. (1995) reported three oxygen-bearing inclusions in natural SiC from Yakutia, namely one FeMg-silicate grain directly associated to moissanite, a sinoite grain, $Si_2N_2O$, and a crystal of a Light Rare Earth Element (LREE) silicate containing 75wt% of $LREE_2O_3$, both associated to silicide inclusions in SiC. Leung et al. (1996) reported rutile grains included in moissanite in kimberlite at Kimberley. Oleynikov et al. (1987) reported Al-silicate included in moissanite from mafic rocks from Russia. Robinson et al. (2004) reported gehlenite-like composition from a grain included in moissanite from Luobusa, while Gao and Liu (2008) found zircon included in moissanite from a carbonatite xenolith. At the best of our knowledge no association of SiC and oxides has been reported in synthetic SiC literature. The sixth, arguable, criterion of Milton and Vitaliano (1984) of finding *large (over 1 cm) crystal* has not been fulfilled so far.

By analogy with similar findings from kimberlitic (Pankov and Spetius 1990, Leung et al. 1990; Mathez et al. 1995; Shiryaev et al. 2011) and ophiolitic environments (Bai et al. 2000; Robinson et al. 2004; Trumbull et al. 2009; Yang et al. 2011), a natural origin of the Turkish moissanite was proposed, mainly based on presence of silicon and Fe-silicide inclusions (Di Pierro et al. 2003). A subsequent carbon isotope study confirmed that the moissanites have $\delta^{13}C$ values typical of other occurrences from the deep mantle (Trumbull et al. 2009).

Here we report the discovery of eight different LREE- and Ba-bearing Ca-Al-silicates (CAS) and Al-silicates (AS), found as hundred-μm grain-sized inclusions in moissanite from Turkey (Di Pierro et al. 2003). We will show that from a thermodynamic point of view the observed Ca-Al mineral association can neither be stable under ambient pressure conditions of

the Acheson process nor any other industrial way of producing silicon-carbide (Knippenberg 1963; Gauthier 1978; Jepps and Page 1983; Lindstad 2002). Zhou and Telle (2010), in fact, using FactSage software package found that undesired $Al_2O_3$, CaO, $Fe_2O_3$ and MgO impurities from the Acheson raw materials, can condense as anorthite, gehlenite, krotite, $CaAl_2O_4$, wollastonite and mullite, in areas at temperatures below 1500° C during the run, while in the internal and hotter part of the Acheson reactor above 1900° C, where α-SiC modifications are stable, elementary Al, Ca, Fe and Mg are present in the gas form.

## SAMPLE AND METHODS

As described in Di Pierro et al. (2003), the here-reported rock is one unique specimen found at beach by Salvatore Musacchia, around 150 km NW from Izmir, Turkey. The source outcrop having not been found so far, the sample is thought to be derived from Tertiary volcanic rocks outcropping in the area (e.g., Innocenti et al., 2005; Aldanmaz et al., 2006). The sample shows a bulk bluish color and consists of a very fine-grained mixture of brucite, phlogopite, calcite and magnesite, in which abundant macrocrysts of quartz and moissanite occur.

Besides optical microscopy, electron microprobe analyses (EMPA) have been performed at the Institute for Geology, University of Bern using a Cameca SX 50 microprobe, wavelength dispersive spectrometers (WDS), and operating conditions of 15 kV and 20 nA. Natural and synthetic silicate and oxide standard were used: almandine (Fe), olivine (Mg), orthoclase (K, Si), anorthite (Ca, Al), eskolaite (Cr), tephroite (Mn), albite (Na), ilmenite (Ti) and bunsenite (Ni). Detection limits in element wt% are: Si 0.02; Ti 0.03; Zr 0.04; Na 0.03; Al 0.02; Y 0.06; Ce 0.08; La 0.08; Fe 0.07; Mn 0.08; Mg 0.03; Ca 0.02; Sr 0.07; Ba 0.08; K 0.02; Na 0.03; S 0.03; F 0.13

and Cl 0.04. Additional analyses were obtained at the University Claude Bernard Lyon-1 and Ecole Normale Supérieure (ENS) of Lyon (Joint Laboratory of Earth Sciences), operating conditions of 15 kV and 20 nA.

Raman spectra were recorded with a DILOR XY spectrometer equipped with confocal optics and a nitrogen-cooled CCD detector, at the ENS-Lyon. A microscope has been used to focus the excitation laser beam (514 nm lines of a Spectra Physics® Ar+ laser) to a 2 μm spot and to collect the Raman signal in the backscattered direction. Collecting times were 20 to 60 s at low power of 2-30 mW, to avoid sample deterioration (not observed during spectra acquisition).

X-ray mapping was performed with a energy dispersive system (EDS) on a Jeol 7600F Scanning Electron Microscope (SEM) using an acceleration voltage of 15 keV conditions, at Saint-Gobain Recherche.

## CHARACTERIZATION OF CAS PHASES

In a polished thin section containing 341 moissanite crystals, CAS inclusions have been observed in at least 21 grains (~6%). Hosting silicon-carbide crystals are *6H*, *15R* or *4H* polytypes.

Ca-Al-silicates and Al-silicates are coarse-grained, up to 150 μm in length, tabular or xenomorphic, or drop-like in shape (Figs. 1–3) and found as inclusions or in oriented contact with moissanite crystals.

In reflected light and in BSE images, CAS and AS phases show different shades of grey while they normally show either very-low or no birefringence (Fig. 1). They are mainly included in moissanite crystals, but some are growing on SiC boundaries (Fig. 1). They occur also associated to silicon and Fe-Ti-Al-Ca-silicide inclusions in moissanite (Fig. 1). Most CAS

inclusions present exsolution textures, consisting of 10-20 μm wide and maximally 50 μm long dark and bright lamellae, intersecting at low angles (Figs. 2-3). Point counting shows that the two exsolved phases occupy each about 50 vol.% of the Ca-Al inclusions.

Microprobe analyses of CAS crystals have been carried out in fourteen moissanite grains and representative analyses are compiled in Table 1. Compositions are somewhat variable but at least eight different compounds can be distinguished.

The most common type of CAS inclusion consist of an association of dark lamellae of stoichiometric $CaAl_2Si_2O_8$ (Table 1) and bright lamellae of an unreported, apparently stoichiometric, $Ca_x(Al,Si)_{1-x}O_3$ phase (Table 1; Fig. 2). About 1-2 mol% of "celsiane"-component is found in the $CaAl_2Si_2O_8$ structure, which is also SrO-, $SO_2$- and LREE-bearing (up to 0.30 wt%; Table 1). $CaAl_2Si_2O_8$ shows main Raman modes at **120**, 225, **330**, **442**, 508, 807, 897, **917** and 1126 $cm^{-1}$ (in bold the strongest ones, see Fig. 4a), which corresponds to the pseudo-hexagonal polymorph (Daniel et al. 1995) named *dmisteinbergite* (Jambor and Vanko 1992; Sokol et al. 1998). Dmisteinbergite was also observed as the only mineral present in some inclusions. $Ca_x(Al,Si)_{1-x}O_3$ can contain up to 40.18 wt% of $Al_2O_3$, while it is also BaO-, SrO-, $SO_2$-, and LREE-bearing (up to 0.33 wt%; Table 1). This phase shows main Raman modes at 175, **416**, **1009** and 1136 $cm^{-1}$ (Fig. 4b).

In a second association, *dmisteinbergite* occurs associated in a bright and dark lamellae structure with stoichiometric $Ca_{1-x}(Al,Si)_{2+x}O_5$ (Table 1; Fig. 3). This phase can accommodate up to 21.84 wt% of $Al_2O_3$, while it is also BaO-, $SO_2$-, LREE- (up to 2.05 wt%), F- (up to 3.91 wt%) and Cl-bearing (Table 1). No detectable Raman modes are active for $Ca_{1-x}(Al,Si)_{2+x}O_5$ phase. It has also been found in contact to TiN (osbornite; Fig. 3).

Stoichiometric, Mg- and Fe-free, but BaO-, SrO-, and $SO_2$-bearing *gehlenite*, $Ca_2Al_2SiO_7$ (Table 1) has been found bordering three moissanite crystals. The studied *gehlenite* shows Raman

165 modes at 182, 221, 248, **310**, **632**, 658, 798, **914**, 982 and 1009 $cm^{-1}$ (Fig. 4c), which fits
166 literature data (Sharma et al. 1983; Bouhifd et al. 2002). Gehlenite-like composition has been also
167 reported from a grain included in moissanite from Luobusa (Robinson et al., 2004).

168 Four other CAS and AS compositions have been measured with the microprobe, either
169 occurring as single inclusions or associated to *dmisteinbergite*.

170 The first mineral is a silica-bearing Ca-aluminate, with the stoichiometry of $CaAl_{4-x}Si_xO_7$.
171 The mineral is also BaO-, SrO-, and $SO_2$-bearing (Table 1) and shows weak Raman modes at
172 118, 138, 252, 303, 326, 412, 458 and 1125 $cm^{-1}$. The mineral is compositionally comparable to
173 grossite, $CaAl_4O_7$ (e.g., Boyko and Wisnyi 1958: Weber and Bischoff 1994) but the Raman
174 spectrum obtained is not in agreement with data reported by Hofmeister et al. (2004).

175 A second CAS phase has a composition of $Ca_{1-x}(Al,Si)_{3+x}O_6$, close to that of the pyroxene
176 kushiroite, $CaAl_2SiO_6$. This phase also contains BaO, SrO, $SO_2$ and traces of LREE (Table 1). It
177 shows weak Raman modes at 239, 291-301, 326-347, 546-548, 604, 622-626 and 966 $cm^{-1}$ on
178 one grain, and strong Raman modes at **531** and **1579** $cm^{-1}$ on a second grain (Fig. 4d).

179 The third unreported CAS phase has a $Ca_{3-x}(Al,Si)_{6+x}O_{14}$ composition. This phase also
180 bears BaO, SrO, $SO_2$ and $Ce_2O_3$ (Table 1), and shows main Raman modes at 351, **553** and 613
181 $cm^{-1}$ (Fig. 4e).

182 The fourth phase, included as single grain within a moissanite crystal, is an Al-silicate;
183 $SiO_2$ averages 65.9 wt%, while $Al_2O_3$ averages 17.4 wt%; the phase also contains 3 wt% alkalis,
184 6 wt% BaO, 2 wt% $SO_2$, less than 2 wt% CaO+MgO, almost 0.9 wt% $ZrO_2$ and up to 0.53 wt%
185 LREE (Table 1). This phase shows main Raman modes at 147, 216, 283, 314, **461**, 535, 576, 671,
186 984, 1136, 1450 and 1524 $cm^{-1}$ (Fig. 4f), with the strongest peak at **461** $cm^{-1}$, close to that of
187 quartz. Oleynikov et al. (1987, Table 2, p.158) reported Mg-free alumina-silicate phase with a
188 very similar composition, namely (microprobe data) $SiO_2$ 78.80-93.17wt%, $Al_2O_3$ 3.05-

189 11.26wt%, $K_2O$ 0.77-5.15wt%, $Na_2O$ 0.48-1.98wt%, CaO 0.19-0.41wt%, FeO 0.21-0.74wt% and
190 $TiO_2$ 0.09-0.35wt%. This hundred μm-sized, tabular phase, along with silicides, was found
191 included in moissanite from heavy-mineral separates from mafic rocks from Russia.

192 In summary, the tabular, xenomorphic, or drop-shaped, hundred-μm sized CAS and AS
193 inclusions in moissanite show exsolution lamellae of the following types: 1) *dmisteinbergite*
194 (hexagonal modification of $CaAl_2Si_2O_8$; n=15), in association with either $Ca_x(Al,Si)_{1-x}O_3$ (n=8)
195 or $Ca_{1-x}(Al,Si)_{2+x}O_5$ (n=4), or even *dmisteinbergite* alone; 2) *gehlenite* (n=3); (simplified) $CaAl_{4-x}Si_xO_7$
196 (n=1); $Ca_{1-x}(Al,Si)_{3+x}O_6$ (n=5); $Ca_{3-x}(Al,Si)_{6+x}O_{14}$ (n=3) and Al-bearing $SiO_2$ (n=1), mainly
197 as single minerals, either included in, or rimming moissanite crystals. All CAS phases are
198 variably enriched in Ba, Sr, S, LREE and Zr (Table 1), and most of them show distinctive Raman
199 modes and spectra.

200 MgO and FeO contents are in all analyzed CAS phases at or below the detection limit,
201 with maximum MgO contents of 0.75 wt% in one analysis of *dmisteinbergite*, and maximum FeO
202 content of 0.39 wt% in another *dmisteinbergite* analysis. This is coherent with literature data
203 predicting iron-free silicates in equilibrium with SiC (Mathez et al. 1995; Ulmer et al. 1998).
204
205 **DISCUSSION**
206
207 The data demonstrate that the CaAl-silicates inclusions hosted in moissanite crystals
208 cannot be synthetic because of the thermodynamic incompatibility between the α-modification of
209 SiC, above 1900° C, and condensation temperatures of potentially present CAS phase, below
210 1500° C (Zhou and Telle 2010). Moreover, most of the analyzed CAS phases included in
211 moissanite are LREE-bearing, in some cases also fluorine-bearing. This is definitely not

compatible with the Acheson synthesis conditions. One particular phase, containing >66 wt% $SiO_2$ and showing a close-to-quartz Raman spectrum (Fig. 4f), might have existed in the Acheson mixture at room conditions, but could not have survived as inclusion within SiC without having been reduced to carbide or silicide. As already stated, neither CAS nor any kind of oxides is reported from the synthetic SiC literature. The only phases reported in synthetic material are silicides, boron-carbides and amorphous carbon precipitates (e.g., More et al. 1986; Backhaus-Ricoult et al. 1993; Munro 1997).

The association of CAS phases as inclusions in moissanite opens new questions about the P-T conditions of formation. Given that our moissanite occurrence is comparable to occurrences in kimberlites and other diamond-bearing assemblages (see introduction), it is obvious to claim pressure as the stabilizer "ingredient" of the observed CAS association. We will therefore review whether the here-reported CAS phases are ultrahigh-pressure phases.

**The $CaO – Al_2O_3 – SiO_2$ system**

The liquidus surface of the well-studied ternary $CaO$-$Al_2O_3$-$SiO_2$ system (e.g., Osborn and Muan 1960; Mao et al. 2006) at ambient-pressure is shown in figure 5. The plotted points are analyses of CAS phases found in this study, in wt%. Coexisting phases are connected with tie lines.

*Gehlenite* analyses plot in the stability field of gehlenite and *dmisteinbergite* in the stability field of anorthite, while all the other compositions do not fit any of the ambient pressure stability fields. These latter are therefore either quenched melt inclusion, or they represent high-pressure (*HP)* phases that may have crystallized from melt inclusions. The former option can be discarded because $Ca_x(Al,Si)_{1-x}O_3$, $Ca_{1-x}(Al,Si)_{3+x}O_6$, $Ca_{3-x}(Al,Si)_{6+x}O_{14}$ and the Al-bearing $SiO_2$

phases show active Raman modes with sharp peaks (Fig. 4), indicative of crystallinity. However, not all Raman spectra (Fig. 4) do fit known phases in the CAS system.

*Dmisteinbergite* was found in pyrometamorphic rocks from the Chelyabinsk coal basin, Southern Urals (Sokol et al. 1998), in pseudotachylyte from the Gole Larghe Fault, Italian Alps (Nestola et al. 2010), and very-recently also from the Allende meteorite (Ma et al. 2013). *Dmisteinbergite* crystallizes from a rapidly quenched silicate melt at ambient pressure at 1200-1400°C instead of *anorthite* (Abe et al. 1991; Daniel et al. 1995). It is not clear whether very-low oxygen-fugacity conditions help stabilizing the meta-stable hexagonal and orthorhombic $CaAl_2Si_2O_8$ polymorphs (Sokol et al. 1998, and reference therein). The upper *P* stability limit of *dmisteinbergite* is not reported in the literature.

*Anorthite* has been used as starting material in numerous *HT-HP* experiments aimed at characterizing Ca-Al-silicate stability in the upper mantle (see below). *Anorthite* remains stable up to 17.5 GPa and 1500° C (Gautron and Madon 1994), above which it decomposes to an assemblage of "distorted" *anorthite* with an hollandite-type *HP* structure, Al-rich $CaSiO_3$ with a perovskite-structure and *kyanite*, according to the following reaction:

$$CaAl_2Si_2O_8 \rightarrow Ca_{1.33}Al_{1.33}Si_{2.33}O_8 + (Ca_{0.80},Al_{0.20})(Si_{0.80},Al_{0.20})O_3 + Al_2SiO_5 \quad [1]$$

*Gehlenite* is a highly refractory mineral occurring in *HT* metamorphic peralumineous rocks that underwent calcium metasomatism and *HT* contact aureoles in impure limestone. The nearly pure, Fe- and Mg-free end-member has mainly been reported from carbonaceous chondrites (e.g., Zhang and Hsu 2009; Simon and Grossman 2011). Experimental work has shown that the assemblage *gehlenite*, *anorthite* and liquid, is stable up to 2.5 GPa and 1400° C, above which it breaks down to *grossular*, $Ca_3Al_2Si_3O_{12}$ (Surkov and Doroshev 1998).

*Grossular* has been also extensively used as a starting material in *HP-HT* experiments, recently reviewed by Kawai and Tsuchiya (2012), to constrain stability fields of Ca- and Al-

hosting silicates in subducted sediments and continental rocks down to upper mantle and greater depths. Ahmed-Zaïd and Madon (1995) used a diamond anvil cell (DAC) and transmission electron microscopy (TEM) to study the breakdown of pure, natural *grossular* at 40 and 50 GPa according to the reaction:

$$Ca_3Al_2Si_3O_{12} \rightarrow 2(Ca_{0.92},Al_{0.08})(Si_{0.92},Al_{0.08})O_3 + CaAl_2SiO_6 \quad [2]$$

Experiments were conducted at temperatures above 1100° ± 400° K. The 8 mol% $Al_2O_3$-bearing $CaSiO_3$ phase was found to be amorphous, while $CaAl_2SiO_6$ was crystalline, but did not show the Ca-Tschermakite pyroxene structure. At estimated temperatures of 2200° ± 800° K, they reported the following reaction:

$$Ca_3Al_2Si_3O_{12} \rightarrow 2CaSiO_3\,(\text{Al-rich}) + Al_2SiO_5 + CaO \quad [3]$$

In these experiments, the 9 mol% $Al_2O_3$-bearing $CaSiO_3$ phase was amorphous, while $Al_2SiO_5$ was a new polymorph with titanite structure, along with crystalline CaO.

Yusa et al. (1995) conducted DAC experiments at 30.2 GPa and 1000-1500° C and reported the appearance of a new, unquenchable garnet polymorph of *grossular* composition, but in-situ X-ray diffraction showed that the phase has a *Pbnm* orthorhombic symmetry comparable to $MgSiO_3$ perovskite.

Takafuji et al. (2002) used a multi-anvil press (MAP) coupled to synchrotron μ-XRD and analytical TEM to study in-situ and quenched reaction products of synthetic *grossular* at 23-25 GPa and 1000-1600° K. In the quenched experiments, they found different associations of 8-25 mol% of an $Al_2O_3$-bearing $CaSiO_3$ phase alternating with lamellae of amorphous material and a "$LiNbO_3$-type" perovskite-structured phase. The authors noted that the Al solubility in $CaSiO_3$-perovskite decreased with increasing temperature (see also Kurashina et al. 2004; Komabayashi et al. 2007), and suggested that under unquenched conditions the amorphous phase had cubic symmetry, while the "$LiNbO_3$-type" was orthorhombic.

283 By studying the potential incorporation of uranium and thorium in silicates at mantle *P-T*
284 conditions and using glass of *grossular* composition as starting material, Gréaux et al. (2009;
285 2011a; 2012) carried out DAC and MAP experiments at 19-26 GPa and 700-2000° K. Run
286 products were characterized either in-situ by μ-XRD or in quenched experiments by TEM.
287 Gréaux and co-workers produced Al-rich $CaSiO_3$ perovskite containing 10.6-24.2 wt% $Al_2O_3$. In
288 their runs, excess alumina was accommodated in the *CAS-phase* $CaAl_4Si_2O_{11}$.

289 $CaAl_4Si_2O_{11}$ was first reported by Irifune et al. (1994) while studying the decomposition
290 of continental sediments at *P-T* conditions of the Transition Zone. Hirose et al. (1999) found as a
291 liquidus phase of mid-ocean ridge basalt (MORB) exposed to 26-27 GPa and approximately
292 2500° K, respectively. A related Na-bearing CAS-phase, $(Ca_xNa_{1-x})Al_{3+x}Si_{3-x}O_{11}$, was also
293 reported as natural mineral occurring in melt pockets of the heavily shocked Martian meteorite
294 NWA 856 (Beck et al. 2004). Zhai and Ito (2008) studied the *P-T* stability of this *CAS-phase* at
295 10-23 GPa and 1000-1600° C. $CaAl_4Si_2O_{11}$ was found stable above 10 GPa and 1500° C, with
296 the boundary of its breakdown products *grossular* + *corundum* + *stishovite* showing a negative
297 d*P*/d*T* slope. The upper stability of $CaAl_4Si_2O_{11}$ lies at approximately 30 GPa and 2000° K,
298 where it dissociates to an assemblage of Al-rich $CaSiO_3$ with perovskite structure, *corundum* and
299 *stishovite* (Ishibashi et al. 2008; Gréaux et al. 2011b). Gautron et al. (1999) refined the structure
300 of their *CAS-phase* as $CaAl_4Si_2O_{11}$ and found it isostructural with $BaFe_4Ti_2O_{11}$.

301 Another important *HP-HT* CAS-phase is $CaAl_{12}Si_4O_{27}$, experimentally synthetized at 14
302 GPa and 1550° C by Grey et al. (2000). Grey et al. (2000) considered their CAS-phase
303 $CaAl_{12}Si_4O_{27}$ to be isostructural with $BaFe_{11}Ti_3O_{23}$. These latter authors suggested that the BaO-
304 $Fe_2O_3$-$TiO_2$ ambient pressure system might be an analogue to the CaO-$Al_2O_3$-$SiO_2$ high-pressure
305 one, where the silicon is six-fold coordinated in a rutile-type structure. Given the complexity of
306 the BaO-$Fe_2O_3$-$TiO_2$ system with at least seventeen known phases (Vanderah et al. 1996, and

307 reference therein), there is still a high probability to find additional new phases in the *HP* CaO-
308 $Al_2O_3$-$SiO_2$ system (Gautron et al. 1999; Grey et al. 2000).

309 The Al-poor *HP-HT* $CaSiO_3$ system is rather well constrained too (Kanzaki et al. 1991;
310 Wang and Weidner 1994; Gasparik et al. 1994; Swamy and Dubrovinsky 1997; Shim et al. 2000;
311 Akaogi et al. 2004; Komabayashi et al. 2007). *LP-HT wollastonite*, $CaSiO_3$, and its *HT*
312 polymorph *pseudo-wollastonite*, $Ca_3Si_3O_9$, (Seryotkin et al. 2012) undergo displacive phase
313 transition to $Ca_3Si_3O_9$ with walstromite-structure at around 3-4 GPa (Joswig et al. 2003; Barkley
314 et al. 2011; Liu et al. 2012). With increasing pressure, walstromite-structured $Ca_3Si_3O_9$
315 dissociates at 9-11 GPa to *larnite*, ß-$Ca_2SiO_4$, and titanite-structured $CaSi_2O_5$ (Angel et al. 1996;
316 Angel 1997; Kudo and Kanzaki 1998; Angel et al. 1999; Stebbins and Poe 1999; Schoenitz et al.
317 2001; Sueda et al. 2006). Larnite and $CaSi_2O_5$ are thought to be important *REE*-carriers at mantle
318 depths (Wang et al. 2000; Dörsam et al. 2009). Experimental work also confirmed the
319 assemblage walstromite-structured $Ca_3Si_3O_9$, *β-larnite* + titanite-structured $CaSi_2O_5$ in natural
320 diamonds from Guinea (Joswig et al. 1999; Stachel 2001; Nasdala et al. 2003; Brenker et al.
321 2005). Above 14-15 GPa and 1600° C, this assemblage further recomposes to more compact
322 $CaSiO_3$ with perovskite-structure.

323 At even higher *P* and by adding alumina to the system, the $CaSiO_3$ perovskite-structured
324 phase is replaced by a rhombohedral $Ca_2AlSiO_{5.5}$ phase that possesses ordered oxygen defects. It
325 is stable at 16 GPa and 1973° K (Bläss et al. 2007; Kojitani et al. 2009).

326 By increasing the $Al_2O_3$/CaO ratio, *kushiroite*, $CaAl_2SiO_6$, a Mg- and Fe-bearing
327 pyroxene containing up to 88 mol% of Ca-tschermakite becomes stable. The Ca-tschermakite
328 end-member *P-T* stability field has been constrained experimentally above 1.8 GPa and 1300° C
329 (Okamura et al. 1974; Ahmed-Zaïd and Madon 1995; Surkov and Doroshev 1998). *Kushiroite*

330 was found in the meteorites ALH 85085 (Kimura et al. 2009), Allende, Murray and other
331 carbonaceous chondrites (Ma et al. 2009) that did not undergo high-pressure metamorphism.
332
333 The Raman spectra of *dmisteinbergite* and *gehlenite* fit those of literature (Nestola et al.
334 2010; Bouhifd et al. 2002). However, a direct link between X-ray characterized *HP-HT* CAS
335 phases and our Raman-constrained data is not yet made. The collected Raman spectra of $Ca_{1-x}(Al,Si)_{3+x}O_6$
336 (Fig. 4d) do not fit that of *kushiroite* (Kimura et al. 2009) nor Ca-tschermakite
337 (Sharma et al. 1983). Similarly, the $CaAl_{4-x}Si_xO_7$ Raman spectra do not fit grossite, $CaAl_4O_7$
338 (Hofmeister et al. 2004).
339 Based on their compositions, however, there are striking analogies between the here-
340 reported CaAl-silicates and the above-reported *HP-HT* phases from the literature. For instance,
341 the $Ca_x(Al,Si)_{1-x}O_3$ phase reported here contains up to 25 mol% of $Al_2O_3$ (Table 1), which
342 corresponds to the maximum solubility of alumina within the perovskite-structured $CaSiO_3$ of
343 Takafuji et al. (2002) or Gréaux et al. (2009; 2011a-b). $Ca_{1-x}(Al,Si)_{3+x}O_6$ compositions reported in
344 Table 1 are closely stoichiometric Ca-tschermakite. The $Ca_{1-x}(Al,Si)_{2+x}O_5$ phase, which contain up
345 to 2 wt% REE, ~3% BaO and ~4 wt% F, >1.7 wt% $SO_2$ and 0.34 wt% $ZrO_2$ is comparable to the
346 data and predictions of Dörsam et al. (2009) suggesting that these phase can be the mantle
347 depository for large ion lithophile elements (*LILE*) and *LREE*. Our $Ca_{3-x}(Al,Si)_{6+x}O_{14}$ phase,
348 furthermore, written with its actual stoichiometry derived from its microprobe analysis (Table 1,
349 #65), namely $Ca_{2,55}Al_{2,60}Si_{3,74}O_{14}$, might recall closely phase $Ba_3Fe_2Ti_4O_{14}$ reported by Vanderah
350 et al. (1996) and refined in the *C2/m* space group, with which it might be iso-structural. Likewise
351 the *HP* phases $CaAl_{12}Si_4O_{27}$ of Grey et al. (2000) is isostructural with $BaFe_{11}Ti_3O_{23}$, and
352 $CaAl_4Si_2O_{11}$ of Gautron et al. (1999) is isostructural with $BaFe_4Ti_2O_{11}$ (see previous discussion).

353 The short review provided above considered single, stoichiometric, either quenched or in-
354 situ equilibrated minerals. We recall that the here-reported CAS inclusions in moissanite mainly
355 consist of two phases, where one phase forms exsolution lamellae in a second. In the literature
356 (i.e., Takafuji et al. 2002; Yamamoto et al. 2009; Gréaux et al. 2011a-b; Nishi et al. 2011) such a
357 textural relationship is interpreted as retrograde transformation in association with volumetric
358 changes occurring during upwelling and decompression (e.g., Alifirova et al. 2012, and reference
359 therein).

360 This, in turn, means that the parental minerals which transformed to the here observed
361 associations (modal abundance in brackets): (a) *dmisteinbergite* (~50 vol.%) + $Ca_x(Al,Si)_{1-x}O_3$
362 (~50 vol.%; Fig. 2), (b) or *dmisteinbergite* (~50 vol.%) + $Ca_{1-x}(Al,Si)_{2+x}O_5$ (~50 vol.%: Fig. 3)
363 should have been even denser phases, whose stoichiometry might be found within the *HP-HT*
364 $CaO$-$Al_2O_3$-$SiO_2$ system.

365 Further combined structural and Raman studies of the presented phases, as well as
366 experimental work on hypothetical compositions are strongly needed in order to explore the CaO-
367 $Al_2O_3$-$SiO_2$ system at high pressures.

368

369 **Hypotheses on moissanite and CAS origins**

370 Several findings of moissanite have been reported, either as genetically linked to sub-
371 surface phenomena, such as impact craters (i.e., Moissan 1905; Hough et al. 1995) or forest fires
372 (Sameshima and Rodgers 1990), or predicted as a thermodynamically stable phase growing
373 during lightning strikes (Essene and Fisher 1986). Most moissanite occurrences, however, have
374 been reported from rocks of deep-mantle provenance, such as kimberlites, lamproites and
375 peridotites (ophiolites), and their narrow association with diamonds has been unambiguously
376 proved (Mathez et al. 1995; Trumbull et al. 2009; Shiryaev et al. 2011, and references therein).

Although authors often speculate about the enigmatic and unsolved origin of natural, terrestrial silicon-carbide, there is a general strong consensus on two points:

(1) Moissanite stability is restricted to extremely low oxygen fugacity ($fO_2$) conditions, computed or experimentally determined at five to six log units below the iron-wüstite (IW) oxygen buffer (Essene and Fisher 1986; Mathez et al. 1995; Ulmer et al. 1998; Dobrizhinetskaya and Green II 2007; Takahashi et al. 2013; Shiryaev and Gaillard 2014; Schmidt et al, 2014).

(2) Moissanite shows strongly depleted $\delta^{13}C$ values, ranging from -18 to -35‰ for ophiolite suites, from -21 to -31‰ for the Turkish pebble suite (Trumbull et al. 2009), and from -22 to -30‰ for the kimberlitic suites of Marshintsev (1990), Leung et al. (1990) and Mathez et al. (1995). These values are in strong contrast with $\delta^{13}C$ values of peridotitic and the large majority of eclogitic diamond suites (Shirey et al. 2013), plotting around -5‰ and considered as the "normal" mantle range. The moissanite values, instead, better fit the $\delta^{13}C$ values of diamonds from ophiolites, ranging -18 to -28‰ (Yang et al., 2014). These diamonds, very-often associated to moissanite, are interpreted as originated from the Transition Zone (Yang et al., 2014).

Based on these facts, a number of hypotheses for a deep-mantle origin of moissanite and hence also the CAS and AS inclusions in moissanite they contain is proposed. Mathez et al. (1995) proposed that moissanite might have an upper mantle origin, where it might be confined to microenvironments with $fO_2$ conditions lower than IW values. They also proposed that the origin of moissanite might be genetically linked to subduction of biogenic carbon. This scenario would be consistent with the C and N isotopes signature, while reducing conditions necessary for SiC formation would be provided by serpentinization processes (Mathez et al. 1995; Ulmer et al. 1998).

399 *Moissanite with CAS inclusions could have a pristine origin from primordial Earth and*
400 *would be located mostly in the Lower Mantle*. This hypothesis was first raised by Mathez et al.
401 (1995) based on the assumptions that Earth Core formation required lower-than-IW $fO_2$
402 conditions (see also Hin et al., 2014), that current $fO_2$ conditions of the lower mantle are not well-
403 known, and that H- and L-ordinary chondrites and achondrites show $\delta^{13}C$ values of -20 to -32‰.
404 The pristine moissanite origin hypothesis has been also suggested by Hugh Rollinson (pers.
405 comm. 2009, in Trumbull et al. 2009), based on analogy of $\delta^{13}C$ values of 12 Martian meteorites
406 of -20 ± 4‰ (Grady et al. 2004) and the average values of terrestrial moissanite. This scenario
407 was recently supported by Horita and Polyakov (2015) using carbon budget modeling.
408 More recently, Hazen et al. (2013) proposed that moissanite might have formed during the
409 giant impact formation of the Earth's Moon since mantle material was exposed to vacuum of
410 space, simultaneously to very *HT* regimes.
411 Even though we still miss many experimental data to constrain with certainty the high-
412 pressure origin of the moissanite-bearing phases studied here, Ca-Al-silicates found as inclusions
413 in SiC described in this study are a unique proxy to tentatively explain a possible origin. We
414 speculated about their *HP-HT* origin already, but there is another striking feature that
415 characterizes the association of CAS-phases with SiC. All analyzed phases are unexpectedly Mg-
416 free. Moissanite, silicon metal and iron-silicides previously characterized in the same sample (Di
417 Pierro et al. 2003) are all also Mg-free. This strongly contrasts with the surrounding brucite-
418 dominated groundmass of the sample, crowded with MgFe-silicates and chromian spinel. This
419 would suggest that the reduced phases, moissanite, silicon and silicides, and associated Mg-free
420 CaAl-silicates form a separate paragenesis, possibly not in equilibrium with the surrounding
421 ultramafic matrix.

*Dmisteinbergeite* (Ma et al. 2013), *kushiroite* (Kimura et al. 2009), and *ghelenite* (Nomura and Miyamoto 1998; Krot et al. 2004; Zhang and Hsu 2009; Simon and Grossman 2011), have all been extensively reported from Ca-Al-inclusions (CAIs) in chondrites, and were interpreted as pristine minerals witnessing the early stages of formation of the Solar System. Moreover, traces of μm-sized, cubic silicon-carbide grains of presolar origin have been extensively reported from carbonaceous chondrites as well (see Daulton et al., 2002, for a review). One could therefore speculate that during the early accretion steps of our planet, significant traces of refractory moissanite and CaAl-silicates might have coexisted (Hazen et al. 2008; Marakushev et al. 2013) and become commonly scattered at different mantle depths. Kimberlite-like volcanism might have ultimately brought up to surface these double, composite parageneses. This scenario would fit simultaneously the previously listed constraints such as the-lower-than-IW $fO_2$ conditions, the strongly depleted $\delta^{13}C$ values not fitting the mantle values of peridotitic and most of eclogitic diamonds but those of pristine meteorites. However, moissanite grains are only known from unequilibrated primitive chondrites but not from higher grade metamorphic, equilibrated chondrites (Brearley and Jones 1998). For this reason, it seems thermodynamically impossible that such tiny moissanite grains of meteoritic origin could have survived in the hot terrestrial mantle.

The Si isotope distribution between moissanite, silicon metal and silicides, and of course CAS phases, would be helpful to discern between a common origin or not for this association, and REE pattern of the CaAl-silicates could be helpful to support such a scenario (Shiryaev et al. 2011).

## IMPLICATIONS

445 Hundred-µm sized grains consisting of crystalline Ca-Al-silicates and Al-silicates have been
446 found as inclusions in moissanite that has lower mantle $\delta^{13}C$ isotopic signature (Trumbull et al.
447 2009; Horita and Polyakov, 2015), providing an additional criterion to distinguish natural
448 moissanite from synthetic SiC.
449 A deep-mantle origin is supported by the fact that together with dmisteinbergite and gehlenite,
450 the unreported phases $Ca_x(Al,Si)_{1-x}O_3$, $Ca_{1-x}(Al,Si)_{3+x}O_6$, $Ca_{1-x}(Al,Si)_{2+x}O_5$, $CaAl_{4-x}Si_xO_7$, $Ca_{3-}$
451 $_x(Al,Si)_{6+x}O_{14}$ and Al-bearing $SiO_2$ are found. The exsolution relationship, moreover, indicates
452 that the parental minerals might have been even denser phases of the CAS system. Moreover,
453 there are striking analogies between the CAS inclusions and *HP-HT* CAS phases reported in the
454 literature. Whereas significant amounts of Ba, S, LREE, and in some of them also F, Cl, alkalies
455 and Zr, may have stabilized the CAS-phases to lower pressure conditions, they confirm
456 predictions of Dörsam et al. (2009) that such minerals could be important sinks for LREE and
457 LILE in the deep mantle.
458 Several high-pressure phases of the $CaO-Al_2O_3-SiO_2$ system are isostructural (e.g., Grey et al.
459 2000) with one of the seventeen known members of the low-pressure $BaO-Fe_2O_3-TiO_2$ system
460 (e.g., Vanderah et al. 1996). Considering that in the studied sample alone five unknown minerals
461 of the $CaO-Al_2O_3-SiO_2$ system are present, it seems likely that exploration of the $CaO-Al_2O_3-$
462 $SiO_2$ at high pressure will lead to the discovery of additional CAS phases.
463
464 **Acknowledgments:** Salvatore Musacchia, the person who found the bluish pebble, is greatly
465 acknowledged for providing the material for research. Electron-microprobe analyses at the
466 University of Bern were supported by Schweizerischer Nationalfonds (credit 21-26579.89).
467 Financial support from the Swiss National Science Foundation Commission of the University of

Fribourg (fellowship n. PBFR2-101389) to SDP when he was Post-Doc fellow at ENS/Lyon is greatly acknowledged. We thank Bruno Reynard, Isabelle Daniel and Gilles Montagnac at ENS/Lyon for discussions and Raman lab assistance, and Philippe Grandjean at University Claude Bernard Lyon-1 for WDS-microprobe assistance. Jessy Gillot at Saint-Gobain Recherche is also thanked for the SEM-EDS X-ray mapping of CAS. We also thank Ed Mathez, an anonymous reviewer, and Associate Editor Daniel Hummer for their constructive reviews.

## Reference cited

Abe, T., Tsukamuto, K., and Sunagawa, I. (1991) Nucleation, growth and stability of $CaAl_2Si_2O_8$ polymorphs. Physics and Chemistry of Minerals, 17, 473-484.

Ahmed-Zaïd, I., and Madon, M. (1995) Electron microscopy of high-pressure phases synthesized from natural garnets in a diamond anvil cell: Implications for the mineralogy of the lower mantle. Earth and Planetary Science Letters, 129, 233-247.

Akaogi, M., Yano, M., Tejima, Y., Iijima, M., and Kojitani, H. (2004) High-pressure transitions of diopside and wollastonite: Phase equilibria and thermochemistry of $CaMgSi_2O_6$, $CaSiO_3$ and $CaSi_2O_5$-$CaTiSiO_5$ system. Physics of the Earth and Planetary Interiors, 143-144, 145-156.

Aldanmaz, E., Köprübaşi, N., Gürer, F., Kaymakçi, N., and Gourgaud, A. (2006) Geochemical constraints on the Cenozoic, OIB-type alkaline volcanic rocks of NW Turkey: Implications for mantle sources and melting processes. Lithos, 86, 50-76.

Alifirova, T.A, Pokhilenko, L.N., Ovchinnikov, Y.I., Donnelly, C.L., Riches, A.J.V., and Taylor,

L.A. (2012) Petrologic origin of exsolution textures in mantle minerals: evidence in pyroxenitic xenoliths from Yakutia kimberlites. International Geology Review 54, 1071-1092.

Angel, R.J., Ross, N.L., Seifert, F., and Fliervoet, T.F. (1996) Structural characterization of pentacoordinate silicon in a calcium silicate. Nature, 384, 441-444.

Angel, R.J. (1997) Transformation of fivefold-coordinated silicon to octaedral silicon in calcium silicate, $CaSi_2O_5$. American Mineralogist, 82, 836-839.

Angel, R.J., Kunz, M., Miletich, R., Woodland, A.B., Koch, M., and Knoche, R.L. (1999) Effect of isovalent Si,Ti substitution on the bulk moduli of $Ca(Ti_{1-x}Si_x)SiO_5$ titanites. American Mineralogist, 84, 282-287.

Backhaus-Ricoult, M., Mozdzierz, N., and Eveno, P. (1993) Impurities in silicon carbide ceramics and their role during high-temperature creep. Journal de Physique III, 3, 2189-2210.

Bai, W., Zhous, M., and Robinson, P.T. (1993) Possibly diamond-bearing mantle peridotites and podiform chromitites in the Luobusa and Donqiao ophiolites, Tibet. Canadian Journal of Earth Sciences, 30, 1650-1659.

Bai, W., Robinson, P.T., Fang, Q., Yang, J., Yan, B., Zhang, Z., Hu, X., Zhous, M., and Malpas, J. (2000) The PGE and base-metal alloys in the podiform chromitites of the Luobusa ophiolite, southern Tibet. Canadian Mineralogist, 38, 585-598.

Bai, W., Yang, J., Fang, Q., Yan, B., and Shi, R. (2003) An unusual mantle mineral group in ophiolites of Tibet. Geology in China, 30, 144-150.

Barkley, M.C., Downs, R.T., and Yang, H. (2011) Structure of walstromite, $BaCa_2Si_3O_9$, and its relationship to $CaSiO_3$-walstromite and wollastonite-II. American Mineralogist, 96, 797-801.

Bauer, J., Fiala, J., and Hrichovà, R. (1963) Natural α-silicon carbide. American Mineralogist, 48, 620-634.

Beck, P., Gillet, P., Gautron, L., Daniel, I., and El Goresy, A. (2004) A new natural high-pressure (Na,Ca)-hexaluminosilicate $[(Ca_xNa_{1-x})Al_{3+x}Si_{3-x}O_{11}]$ in shocked Martian meteorites. Earth and Planetary Science Letters, 219, 1-12.

Beckett, J.R., Conolly, H.C., and Ebel, D.S. (2006) Chemical processes in igneous calcium-aluminium-rich inclusions : A mostly CMAS view of melting and crystallization. In *Meteorites and the early solar system II*, edited by Lauretta D. S. and McSween H. Y. Jr.. University of Arizona Press, Tucson, p. 399-429.

Bläss, U.W., Langenhorst, F., Frost, D.J., and Seifert, F. (2007) Oxygen deficient perovskites in the system $CaSiO_3$-$CaAlO_{2.5}$ and implications for the earth's interior. Physics and Chemistry of Minerals, 34, 363-376.

Bouhifd, M.A., Gruener, G., Mysen, B.O., and Richet, P. (2002) Premelting and calcium mobility in gehlenite ($Ca_2Al_2SiO_7$) and pseudowollastonite ($CaSiO_3$). Physics and Chemistry of Minerals, 29, 655-662.

Boyko, E.R., and Wisnyi, L.G. (1958) The optical properties and structures of $CaO \cdot 2Al_2O_3$ and $SrO \cdot 2Al_2O_3$. Acta Crystallographica, A11, 444-445.

Brearley, A.J., and Jones, R.H. (1998) Chondritic meteorites. In Ribbe, P.H. (ed). Planetary materials. Reviews in Mineralogy, 36, 3-1 - 3-398.

Brenker, F.E., Vincze, L., Vekemans, B., Nasdala, L., Stachel, T., Vollmer, C., Kersten, M., Somogyi, A., Adams, F., Joswig, W., and Harris, J.W. (2005) Detection of a Ca-rich lithology in the earth's deep (> 300 km) convecting mantle. Earth and Planetary Science Letters, 236, 579-587.

Daniel, I., Gillet, P., McMillan, P.F., and Richet, P. (1995) An in-situ high-temperature structural study of stable and metastable $CaAl_2Si_2O_8$ polymorphs. Mineralogical Magazine, 59, 25-33.

Daulton, T.L., Bernatowicz, T.J., Lewis, R.S., Messenger, S., Stadermann, F.J., and Amari, S. (2002) Polytype distribution in circumstellar silicon carbide. Science, 296, 1852-1855.

De, S., Heaney, P.J., Hargraves, R.B., Vincenzi, E.P., and Taylor, P.T. (1998) Microstructural observations of polycrystalline diamond: a contribution to the carbonado conundrum. Earth and Planetary Science Letters, 164, 421-433.

Di Pierro, S., Gnos, E., Grobety, B.H., Armbruster, T., Bernasconi, S.M., and Ulmer, P. (2003) Rock-forming moissanite (natural α-silicon carbide). American Mineralogist, 88, 1817-1821.

Dobrzhinetskaya, L., and Green, H.W. (2007) Diamond Synthesis from Graphite in the Presence of Water and $SiO_2$: Implications for Diamond Formation in Quartzites from Kazakhstan. International Geology Review, 49, 389-400.

Dörsam, G., Liebscher, A., Wunder, B., Franz, G., and Gottschalk, M. (2009) Crystal structure

refinement of synthetic $Ca_{0.43}Sr_{0.57}[SiO_3]$-walstromite and walstromite–fluid Ca–Sr distribution at upper-mantle conditions. European Journal of Mineralogy, 21, 705-714.

Essene, E.J., and Fisher, D.C. (1986) Lightning strike fusion: extreme reduction and metal-silicate liquid immiscibility. Science, 234, 189-193.

Gao, C., and Liu, Y. (2008) Moissanite-bearing carbonatite xenoliths from Cenozoic basalt, North China: Products of ancient oceanic crust subduction? Geochimica et Cosmochimica Acta 72(12), p.A292.

Gasparik, T., Wolf, K., and Smith, C.M. (1994) Experimental determination of phase relations in the $CaSiO_3$ system from 8 to 15 GPa. American Mineralogist, 79, 1219-1222.

Gauthier, J. P. (1978) Polytypisme du carbure de silicium: intérêt de la diffraction électronique par réflexion. 161p. Ph.D Thesis, Université Claude-Bernard, France.

Gautron, L., and Madon, M. (1994) A study of the stability of anorthite in the PT conditions of Earth's transition zone. Earth and Planetary Science Letters, 125, 281-291.

Gautron, L., Angel, R.J., and Miletich, R. (1999) Structural characterisation of the high-pressure phase $CaAl_4Si_2O_{11}$. Physics and Chemistry of Minerals, 27, 47-51.

Golovko, A.V., and Kaminsky, F. (2010) The Shoshonite-Absarokite-Picrite Karashoho Pipe, Uzbekistan: An Unusual Diamond Deposit in an Atypical Tectonic Environment. Economic Geology, 105, 825-840.

Grady, M.M., Verchovsky, A.B., and Wright, I.P. (2004) Magmatic carbon in Martian meteorites: attemps to constrain the carbon cycle on Mars. International Journal of

Astrobiology, 3, 117-124.

Gréaux, S., Farges, F., Gautron, L., Trcera, N., Flank, A.M., and Lagarde, P. (2012) X-ray absorption near edge structure (XANES) study of the speciation of uranium and thorium in Al-rich $CaSiO_3$ perovskite. American Mineralogist, 96, 100-109.

Gréaux, S., Gautron, L., Andrault, D., Bolfan-Casanova, N., Guignot, N., and Bouhifd, M.A. (2009) Experimental high pressure and high temperature study of the incorporation of uranium in Al-rich $CaSiO_3$ perovskite. Physics of the Earth and Planetary Interiors, 174, 254-263.

Gréaux, S., Nishiyama, N., Kono, Y., Gautron, L., Ohfuji, H., Kunimoto, T., Menguy, N., and Irifune, T. (2011a) Phase transformations of $Ca_3Al_2Si_3O_{12}$ grossular garnet to the depths of the Earth's mantle transition zone. Physics of the Earth and Planetary Interiors, 185, 89-99.

Gréaux, S., Nishiyama, N., Kono, Y., Irifune, T., and Gautron, L. (2011b) P-V-T equation of state of $CaAl_4Si_2O_{11}$ CAS phase. Physics and Chemistry of Minerals, 38, 581-590.

Grey, I.E., Madsen, I.C., Hibberson, W.O., and O'Neill, H.St.C. (2000) $CaAl_{12}Si_4O_{27}$, a new high-pressure phase containing $Al_6O_{19}$ clusters. Journal of Solid State Chemistry, 153, 391-397.

Hazen, R.M., Papineau D., Bleeker W., Downs R.T., Ferry J., McCoy T., Sverjensky, D., and Yang H. (2008) Mineral evolution. American Mineralogist 93, 1693-1720.

Hazen, R. M., Downs, R. T., Jones, A. P., and Kah, L. (2013) Carbon Mineralogy and Crystal Chemistry. Reviews in Mineralogy & Geochemistry 75, 7-46.

591 Hin, R.C., Fitoussi, C., Schmidt, M.W., and Bourdon, B. (2014) Experimental determination of
592 the Si isotope fractionation factor between liquid metal and liquid silicate. Earth and
593 Planetary Science Letters 387, 55-66.

594 Hirose, K., Fei, Y., Ma, Y., and Mao, H.K. (1999) The fate of subducted basaltic crust in the
595 Earth's lower mantle. Nature, 397, 53-56.

596 Hofmeister, A, M., Wopenka, B., and Locock, A. J. (2004) Spectroscopy and structure of
597 hibonite, grossite and $CaAl_2O_4$: Implications for astronomical environments. Geochimica et
598 Cosmochimica Acta, 68, 4485-4503.

599 Horita, J. and Polyakov, V.B. (2015) Carbon-bearing iron phases and the carbon isotope
600 composition of the deep Earth. Proceedings of the National Academy of Sciences, 112, pp.
601 31 – 36.

602 Hough, R.M., Gilmour, I., Pillinger, C.T., Arden, J.W., Gilkes, K.W.R., Yuan, J., and Milledge,
603 H.J. (1995) Diamond and silicon carbide in impact melt rock from the Ries impact crater.
604 Nature, 378, 41-44.

605 Innocenti, F., Agostini, S., Di Vincenzo, G., Doglioni, C., Manetti, P., Savaşçin, M.Y., and
606 Tonarini, S. (2005) Neogene and Quaternary volcanism in Western Anatolia: Magma
607 sources and geodynamic evolution. Marine Geology, 221, 397-421.

608 Irifune, T., Ringwood, A.E., and Hibberson, W.O. (1994) Subduction of continental crust and
609 terrigenous and pelagic sediments: an experimental study. Earth and Planetary Science
610 Letters, 126, 351-368.

611 Ishibashi, K., Hirose, K., Sata, N., and Ohishi, Y. (2008) Dissociation of CAS phase in the

612 uppermost lower mantle. Physics and Chemistry of Minerals, 35, 197-200.

613 Jambor, J.L. and Vanko, D.A. (1992) New mineral names. American Mineralogist, 77, 446-452.

614 Jaques, A.L., Hall, A.E., Sheraton, J.W., Smith, C.B., Sun, S.S., Drew, R.M., Foudoulis, C., and
615 Ellingsen, K. (1989) Composition of crystalline inclusions and C-isotopic composition of
616 Argyle and Ellendale diamonds in Kimberlite and Related Rocks, Volume 2: Their
617 Mantle/Crust Setting, Diamonds and Diamond Exploration; Proceedings of the Fourth
618 International kimberlite conference. Geological Society of Australia Special Publication.
619 966-989. Blackwell Scientific, Cambridge, U.K.

620 Jepps, N.W., and Page, T.F. (1983) Polytypic transformations in silicon carbide. In Crystal
621 growth and characterization of polytype structures. 259-307. Pergamon Press.

622 Joswig, W., Stachel, T., Harris, J.W., Baur, W.H., and Brey, G.P. (1999) New Ca-silicate
623 inclusions in diamonds - tracers from the lower mantle. Earth and Planetary Science Letters,
624 173, 1-6.

625 Kaminsky, F. (2012) Mineralogy of the lower mantle: A review of 'super-deep' mineral
626 inclusions in diamond. Earth-Sciences Reviews, 110, 127-147.

627 Kanzaki, M., Stebbins, J.F., and Xue, X. (1998) Characterization of quenched high pressure
628 phases in $CaSiO_3$ system by XRD and $^{29}Si$ NMR. Geophysical Research Letters, 18, 463-
629 466.

630 Kawai, K., and Tsuchiya, T. (2012) First Principles investigations on the elasticity and phase
631 stability of grossular garnet. Journal of Geophysical Research B: Solid Earth, 117, art. no.
632 B02202.

633 Kimura, M., Mikouchi, T., Suzuki, A., Miyahara, M., Ohtani, E., and El Goresy, A. (2009)
634 Kushiroite, $CaAlAlSiO_6$: A new mineral of the pyroxene group from the ALH 85085 CH
635 chondrite, and its genetic significance in refractory inclusions. American Mineralogist 94,
636 1479-1482.

637 Klein-BenDavid, O., Wirth, R., and Navon, O. (2007) Micrometer-scale cavities in fibrous and
638 cloudy diamonds – A glance into diamond dissolution events. Earth and Planetary Science
639 Letters, 264, 89-103.

640 Komabayashi, T., Hirose, K., Sata, N., Ohishi, Y., and Dubrovinsky, L.S. (2007) Phase transition
641 in $CaSiO_3$ perovskite. Earth and Planetary Science Letters, 260, 564-569.

642 Kojitani, H., Wakabayashi, Y., Tejima, Y., Kato, C., Haraguchi, M., and Akaogi, M. (2009)
643 High-pressure phase relations in $Ca_2AlSiO_{5.5}$ and energetics of perovskite-related
644 compounds with oxygen defects in the $Ca_2Si_2O_6$–$Ca_2Al_2O_5$ join. Physics of the Earth and
645 Planetary Interiors, 173, 349-353.

646 Knippenberg, W.F. (1963) Growth phenomena in silicon carbide. Philips Research Reports, 18,
647 161-274.

648 Krot, A., Fagan, T.J., Keil, K., McKeegan, K.D., Sahijpal, S., Hutcheon, I.D., Petaev, M.I., and
649 Yurimoto, H. (2004) Ca,Al-rich inclusions, amoeboid olivine aggregates, and Al-rich
650 chondrules from the unique carbonaceous chondrite Acfer 094: I. Mineralogy and
651 petrology. Geochimica et Cosmochimica Acta, 68, 2167-2184.

652 Kudoh, Y., and Kanzaki, M. (1998) Crystal chemical characteristics of α-$CaSi_2O_5$, a new high
653 pressure calcium silicate with five-coordinated silicon synthesized at 1500°C and 10 GPa.

654 Physics and Chemistry of Minerals, 25, 429-433.

655 Kurashina, T., Hirose, K., Ono, S., Sata, N., and Ohishi, Y. (2004) Phase transition in Al-bearing
656 $CaSiO_3$ perovskite: implications for seismic discontinuities in the lower mantle. Physics of
657 the Earth and Planetary Interiors, 145, 67-74.

658 Leung, I. S. (1988) Abundant moissanite found in Fuxian diamond pipe, Liaoning, China. 20(7),
659 74, Abstract n.20850. Conference Proceeding

660 ----- (1990) Silicon carbide cluster entrapped in a diamond from Fuxian, China. American
661 Mineralogist, 75, 1110-1119.

662 Leung, I.S., Guo, W., Friedman, I., and Gleason, J. (1990) Natural occurrence of silicon carbide
663 in a diamondiferous kimberlite from Fuxian. Nature, 346, 352-354.

664 Leung, I.S., Taylor, L.A., Tsao, C.S., and Han, Z. (1996) SiC in Diamond and Kimberlites:
665 Implications for Nucleation and Growth of Diamond. International Geology Review, 38,
666 595-606.

667 Liang, F., Xu, Z., Zhao, J. (2014) In-situ moissanite in dunite: Deep mantle origin of mantle
668 peridotite in Luobusa ophiolite, Tibet. Acta Geologica Sinica (English edition), 88, 517-
669 529.

670 Lindstad, L. H. Recrystallization of Silicon Carbide (2002) Department of Materials Technology
671 and Electrochemistry Norwegian University of Science and Technology N-7491
672 TRONDHEIM. Thesis/Dissertation

673 Liu, X., Wang, S., He, Q., Chen, J., Wang, H., Li, S., Peng, F., Zhang, L., and Fei, Y. (2012)

Thermal elastic behavior of $CaSiO_3$-walstromite: A powder X-ray diffraction study up to 900 °C. American Mineralogist, 97, 262-267.

Ma, C., Simon, S. B., Rossman, G. R., and Grossman, L. (2009) Calcium Tschermak's pyroxene, $CaAlAlSiO_6$, from the Allende and Murray meteorites: EBSD and micro-Raman characterizations. American Mineralogist 94, 1483-1486.

Ma, C., Krot, A. N, and Bizzarro, M. (2013) Discovery of dmisteinbergite (hexagonal $CaAl_2Si_2O_8$) in the Allende meteorite: A new member of refractory silicates formed in the solar nebula. American Mineralogist 98, 1368-1371.

Mao, H., Hillert, M., Sellby, M., and Sundman, B. (2006) Thermodynamic assessment of the $CaO$-$Al_2O_3$-$SiO_2$ system. Journal of the American Ceramic Society, 89, 298-308.

Marakushev, A.A., Glazovskaya, L.I., and Marakushev, S.A. (2013) Evolution of the iron-silicate and carbon material of carbonaceous chondrites. Moscow University Geology Bulletin, 68, 265-281.

Marshintsev, V.K. (1990) Nature of silicon carbide in kimberlites rocks of Yakutia. Mineralogiceskiy Zhurnal, 12, 17-26.

Mathez, E.A., Fogel, R.A., Hutcheon, I.D., and Marshintsev, V.K. (1995) Carbon isotopic composition and origin of SiC from kimberlites of Yakutia, Russia. Geochimica et Cosmochimica Acta, 59, 781-791.

McCammon, C., Hutchinson, M., and Harris, J.W. (1997) Ferric iron content of mineral inclusions in diamonds from São Luiz: A view into the Lower Mantle. Science, 278, 434-436.

695 Milton, C., and Vitaliano, D. B. The non-existence of moissanite, SiC (1984) 27th International
696 Geological Congress. 5, 107-108. Conference Proceeding

697 Moissan, H. (1905) Etude du siliciure de carbone de la météorite de Cañon Diablo. Comptes-
698 rendus Académie des Sciences (Paris), 140, 405-406.

699 Moore, R. O., Otter, M. L., Rickard, R. S., Harris, J. W., and Gurney, J. J. (1986) The occurrence
700 of moissanite and ferro-periclase as inclusions in diamond. 16, 409-411. Conference
701 Proceeding

702 Moore, R.O., and Gurney, J.J. (1989) Mineral inclusions in diamond from the Monastery
703 kimberlite, South Africa in Kimberlite and Related Rocks, Volume 2: Their Mantle/Crust
704 Setting, Diamonds and Diamond Exploration; Proceedings of the Fourth International
705 kimberlite conference. Geological Society of Australia Special Publication. 1029-1041.
706 Blackwell Scientific, Cambridge, U.K..

707 More, K.L., Carter, C.H., Bentley, J., Wadlin, W.H., Lavanier, L., and Davis, R.F. (1986)
708 Occurrence and distribution of Boron-containing phases in sintered α-silicon carbide.
709 Journal of the American Ceramic Society, 69, 695-698.

710 Munro, R.G. (1997) Material properties of a sintered α-SiC. Journal of Physical and Chemical
711 Reference Data, 26, 1195-1203.

712 Nasdala, L., Brenker, F. E., Glinnemann, J., Hofmeister, W., Gasparik, T., Harris, J. W., Stachel,
713 T., and Reese, I. (2003) Spectroscopic 2D-tomography: Residual pressure and strain around
714 mineral inclusions in diamonds. European Journal of Mineralogy 15, 931-935.

715 Nestola, F., Mittempergher, S., Di Toro, G., Zorzi, F., and Pedron, D. Evidence of

dmisteinbergite (hexagonal form of $CaAl_2Si_2O_8$) in pseudotachylyte: A tool to constrain the thermal history of a seismic event (2010) American Mineralogist 95, 405-409.

Nishi, M., Kubo, T., Kato, T., Tominaga, A., Funakoshi, K.I., and Higo, Y. (2011) Exsolution kinetics of majoritic garnet from clinopyroxene in subducting oceanic crust. Physics of the Earth and Planetary Interiors, 189, 47-55.

Nomura, K., and Miyamoto, M. (1998) Hydrothermal experiments on alteration of Ca-Al-rich inclusions (CAIs) in carbonaceous chondrites: Implication for aqueous alteration in parent asteroids. Geochimica et Cosmochimica Acta, 62, 3575-3588.

Okamura, F.P., Ghose, S., and Ohashi, H. (1974) Structure and crystal chemistry of Calcium Tschermak's pyroxene, $CaAlAlSiO_6$. American Mineralogist 59, 549-557.

Oleynikov, B.V., Pankov, V.Y., Plaksenko, A.N., and Okrugin, A.V. (1987) Inclusions in moissanite from mafic rocks of cratons. Transactions (Doklady) of the U.S.S.R. Academy of Sciences: Earth Science Sections, 283, 155-159.

Otter, M. L., and Gurney, J. J. (1986) Mineral inclusions in diamonds from the sloan diatremes, Colorado-Wyoming state line kimberlite district, North America. 16, 415-417. Conference Proceeding

----- (1989) Mineral inclusions in diamonds from the Sloan diatremes, Colorado-Wyoming State Line kimberlite district, North America in Kimberlite and Related Rocks, Volume 2: Their Mantle/Crust Setting, Diamonds and Diamond Exploration; Proceedings of the Fourth International kimberlite conference. Geological Society of Australia Special Publication. 1042-1053. Blackwell Scientific, Cambridge, U.K.

737 Osborn, E.F., and Muan, A. (1960) Phase equilibrium diagrams of oxide systems. Plate 2. The
738 system $CaO$-$Al_2O_3$-$SiO_2$. American Ceramic Society, Columbus, Ohio.

739 Pankov, V.Y., and Spetsius, Z.V. (1990) Iron silicide and native silicon inclusions in moissanite
740 from the Sytykan kimberlite pipe. Transactions (Doklady) of the U.S.S.R. Academy of
741 Sciences: Earth Science Sections, 305, 152-155.

742 Perraki, M., and Faryad, S.W. (2014) First finding of microdiamond, coesite and other UHP
743 phases in felsic granulites in the Moldanubian Zone: Implications for deep subduction and a
744 revised geodynamic model for Variscan Orogeny in the Bohemian Massif. Lithos, 202-203,
745 157-166.

746 Qi, X.X., Yang, J.S., Xu, Z.Q., Bai, W.J., Zhang, Z.M., and Fang, Q.S. (2007) Discovery of
747 moissanite in retrogressive eclogite from the Pre-pilot Hole of the Chinese Continental
748 Scientific Drilling Project (CCSD-PP2) and its geological implication. Acta Petrologica
749 Sinica, 23, 3207-3214.

750 Robinson, P.T., Bai, W.J., Malpas, J., Yang, J.S., Zhou, M.F., Fang, Q.S., Hu, X.F., Cameron, S.,
751 and Staudigel, H. (2004) Ultra-high pressure minerals in the Loubusa Ophiolite, Tibet, and
752 their tectonic implications. Geological Society of London, Special Publications, 226, 247-
753 271.

754 Robinson, P.T., Trumbull, R.B., Schmitt, A., Yang, J.S., Li, J.W., Zhou, M.F., Erzinger, J., Dare,
755 S., and Xiong, F. (2015) The origin and significance of crustal minerals in ophiolitic
756 chromitites and peridotites. Gondwana Research, 27, 486-506.

757 Sameshima, T., and Rodgers, K.A. (1990) Crystallography of 6H silicon carbide from

758 Seddonville, New Zealand. Neues Jahrbuch für MIneralogie Monatshefte, 3, 137-143.

759 Schmidt, M.W., Gao, C., Golubkova, A., Rohrbach, A., and Connolly, J.A.D. (2014) Natural
760 moissanite (SiC) – a low temperature mineral formed from highly fractionated ultra-
761 reducing COH-fluids. Progress in Earth and Planetary Science, 1, 1-14.

762 Schoenitz, M., Navrotsky, A., and Ross, N. (2001) Enthalpy of formation of $CaSi_2O_5$ a quenched
763 high-pressure phase with pentacoordinate silicon. Physics and Chemistry of Minerals, 28,
764 57-60.

765 Seryotkin, Y.V., Sokol, E.V., and Kokh, S.N. (2012) Natural pseudowollastonite: Crystal
766 structure, associated minerals, and geological context. Lithos, 134-135, 75-90.

767 Sharma, S. K., Simons, B., and Yoder, H. S. (1983) Raman study of anorthite, calcium
768 Tschermak's pyroxene and gehlenite in crystalline and glassy states. American Mineralogist
769 68, 1113-1125.

770 Shim, S., Duffy, T.S., and Shen, G. (2000) The stability and P-V-T equation of state of $CaSiO_3$
771 perovskite in the Earth's lower mantle. Journal of Geophysical Research, 105, 25955-25968.

772 Shiryaev, A.A., Griffin, W.L., and Stoyanov, E. (2011) Moissanite (SiC) from kimberlites:
773 Polytypes, trace elements, inclusions and speculations on origin. Lithos, 122, 152-164.

774 Shiryaev, A.A., and Gaillard, F. (2014) Local redox buffering by carbon at low pressures and the
775 formation of moissanite – natural SiC. European Journal of Mineralogy, 26, 53 – 59.

776 Shirey, S. B., Cartigny, P., Frost, D. J., Keshav, S., Nestola, F., Nimis, P., Pearson, D. G.,
777 Sobolev, N. V., and Walter, M. J. (2013) Diamonds and the Geology of Mantle Carbon.

778 Reviews in Mineralogy & Geochemistry 75, 355-421.

779 Simon, S.B., and Grossman, L. (2011) Refractory inclusions in the unique carbonaceous
780 chondrite Acfer 094. Meteoritics and Planetary Science, 46, 1197-1216.

781 Sokol, E., Volkova, N., and Lepezin, G. (1998) Mineralogy of pyrometamorphic rocks associated
782 with naturally burned coal-bearing spoil-heaps of the Chelyabinsk coal basin, Russia.
783 European Journal of Mineralogy, 10, 1003-1014.

784 Stachel,T. (2001) Diamonds from the astenosphere and the transition zone. European Journal of
785 Mineralogy, 13, 883-892.

786 Stebbins, J.F., and Poe, B.T. (1999) Pentacoordinate silicon in high-pressure crystalline and
787 glassy phases of calcium disilicate ($CaSi_2O_5$). Geophysical Research Letters, 26, 2521-
788 2523.

789 Sueda, Y., Irifune, T., Yamada, A., Inoue, T., Liu, X., and Funakoshi, K.I. (2006) The phase
790 boundary between $CaSiO_3$ perovskite and $Ca_2SiO_4$ + $CaSi_2O_5$ determined by in situ X-ray
791 observations. Geophysical Research Letters, 33, art. no. L10307.

792 Surkov, N.V., and Doroshev, A.M. (1998) Phase diagram of $CaO$-$Al_2O_3$-$SiO_2$ system at pressures
793 of up to 40 kbar. Russian Geology and Geophysics, 39, 1257-1272.

794 Svisero, D.P. (1995) Distribution and origin of diamonds in Brazil: an overview. Journal of
795 Geodynamics, 20, 493-514.

796 Swamy, V., and Dubrovinsky, L.S. (1997) Thermodynamic data for the phases in the $CaSiO_3$
797 system. Geochimica et Cosmochimica Acta, 61, 1181-1191.

798 Takahashi, S., Ohtani, E., Terasaki, H., Ito, Y., Shibazaki, Y., Ishii, M., Funakoshi, K., and Higo,
799 Y. (2013) Phase relations in the carbon-saturated C-Mg-Fe-Si-O system and C and Si
800 solubility in liquid Fe at high pressure and temperature: implications for planetary interiors.
801 Physics and Chemistry of Minerals, 40, 647-657.

802 Takafuji, N., Yagi, T., Miyajima, N., and Sumita, T. (2002) Study on $Al_2O_3$ content and phase
803 stability of aluminous-$CaSiO_3$ perovskite at high pressure and temperature. Physics and
804 Chemistry of Minerals, 29, 532-537.

805 Trumbull, R.B., Yang, J.S., Robinson, P.T., Di Pierro, S., Vennemann, T., and Wiedenbeck, M.
806 (2009) The carbon isotope composition of natural SiC (moissanite) from the Earth's mantle:
807 New discoveries from ophiolites. Lithos, 113, 612-620.

808 Ulmer, G.C., Grandstaff, D.E., Woermann, E., Göbbles, M., Schönitz, M., and Woodland, A.B.
809 (1998) The redox stability of moissanite (SiC) compared with metal-metal oxide buffers at
810 1773 K and at pressures up to 90 kbar. Neues Jahrbuch für Mineralogie Abhandlungen,
811 172, 279-307.

812 Vanderah, T.A., Loezos, J.M., and Roth, R.S. (1996) Magnetic dielectric oxides: subsolidus
813 phase relations in the BaO : $Fe_2O_3$ : $TiO_2$ system. Journal of Solid State Chemistry, 121, 38-
814 50.

815 Wang, W., Gasparik, T., and Rapp, R.P. (2000) Partitioning of rare earth elements between
816 $CaSiO_3$ perovskite and coexisting phases: Constraints on the formation of $CaSiO_3$
817 inclusions in diamonds. Earth and Planetary Science Letters, 181, 291-300.

818 Weber, D., and Bischoff, A. (1994) Grossite ($CaAl_4O_7$) – a rare phase in terrestrial rocks and

819 meteorites. European Journal of Mineralogy, 6, 591-594.

820 Wilding, M. C., Harte, B., and Harris, J. W. (1991) Evidence for a deep origin for São Luiz
821 diamonds. 2/91, 456-458. Conference Proceeding

822 Xu, S., Wu, W., Xiao, W., Yang, J., Chen, J., Ji, S., and Liu, Y. (2008) Moissanite in serpentinite
823 from the Dabie Mountains in China. Mineralogical Magazine, 72, 899-908.

824 Yamamoto, S., Komiya, T., Hirose, K., and Maruyama, S. (2009) Coesite and clinopyroxene
825 exsolution lamellae in chromites: In-situ ultrahigh-pressure evidence from podiform
826 chromitites in the Luobusa ophiolite, southern Tibet. Lithos, 109, 314-322.

827 Yang, J.S., Xu, X.Z., Li, Y., Li, J.Y., Ba, D.Z., Rong, H., and Zhang, Z.M. (2011) Diamonds
828 recovered from peridotite of the Purang ophiolite in the Yarlung-Zangbo suture of Tibet: A
829 proposal for a new type of diamond occurrence. Acta Petrologica Sinica, 27, 3171-3178.

830 Yang, J.S., Robinson, P.T., and Dilek, Y. (2014) Diamonds in ophiolites. Elements, 10, 127-130.

831 Yusa, H., Yagi, T., and Shimobayashi, N. (1995) A new unquenchable high-pressure polymorph
832 of $Ca_3Al_2Si_3O_{12}$. Physics of the Earth and Planetary Interiors, 92, 25-31.

833 Zhang, A., and Hsu, W. (2009) Refractory inclusions and aluminum-rich chondrules in Sayh al
834 Uhaymir 290 CH chondrite: Petrography and mineralogy. Meteoritics and Planetary
835 Science, 44, 787-804.

836 Zhai, S., and Ito, E. (2008) Phase relations of $CaAl_4Si_2O_{11}$ at high-pressure and high-temperature
837 with implications for subducted continental crust into the deep mantle. Physics of the Earth
838 and Planetary Interiors, 167, 161-167.

 

839 Zhou, L.Y., and Telle, R. (2010) Purifying Mechanism in the Acheson Process - A
840 Thermodynamic Study. Materials Science Forum, 645-648, 41-44.

841

842

843 **Figure captions**

844 **FIGURE 1.** Thin section photos (reflected light) of Ca-Al-silicates (CAS) in contact or forming
845 inclusions in moissanite crystals. (a) SiC #78: system of multiple inclusions. CAS are in grey,
846 metallic Si in white. The grey crystal growing on the left rim is gehlenite (Ghl: analyses 21-24 in
847 Table 1). The crystal above is Dmisteinbergite (Dms: analysis 17 in Table 1). The CAS crystal to
848 the right has $Ca_{1-x}(Al,Si)_{3+x}O_6$ composition. (b) SiC #199: the two grey inclusions of CAS are
849 arrowed. Details of the larger CAS inclusion, along with the EDS X-ray mapping, are presented
850 in figure 2. (c) SiC #85 containing two grey inclusions of CAS. (d) SiC #244 with a CAS crystal
851 (arrowed: analyses 2-4, and 10-11 in Table 1) on the surface, and associated with a TiN grain, in
852 white. Details of this grain, along with the EDS X-ray mapping, are presented in figure 3.

853

854 **FIGURE 2.** X-Ray mapping of CAS inclusion in SiC #199. Dark lamellae in the BSE image are
855 dmisteinbergite, while bright areas have a $Ca_x(Al,Si)_{1-x}O_3$ composition.

856

857 **FIGURE 3.** X-Ray mapping of CAS inclusion in SiC #244. Dark lamellae in BSE image are
858 Dmisteinbergite (Table 1, analyses 10 and 11), while bright areas have a $Ca_{1-x}(Al,Si)_{2+x}O_5$
859 composition (Table 1, analyses 2 to 4).

860

**FIGURE 4**. Raman spectra of Ca-Al-rich phases. (a) Spectra of dmisteinbergite inclusions (Dms), along with that of hosting 4H-SiC. Blue: Pure dmisteinbergite in grain #244; red: dminsteinbergite in association with SiC-4H in grain #85. (b) Mixed spectra of $Ca_x(Al,Si)_{1-x}O_3$, along with that of hosting phase 4H-SiC. Blue: Spectrum obtained in grain #85; red: spectrum obtained in grain #78. (c) Two pure spectra of gehlenite (Ghl) in grain #78 (both, blue and red). (d) Spectrum of $Ca_{1-x}(Al,Si)_{3+x}O_6$. (e) Spectra of $Ca_{3-x}(Al,Si)_{6+x}O_{14}$ phase, along with that of hosting SiC (grain #27). Green: Spectrum displaying a strong moissanite peak and a weaker $Ca_{3-x}(Al,Si)_{6+x}O_{14}$ peak; red: spectrum showing strong peak of $Ca_{3-x}(Al,Si)_{6+x}O_{14}$ and weak moissanite peak; blue: spectrum showing only weak $Ca_{3-x}(Al,Si)_{6+x}O_{14}$ peak. (f) Spectra of Al-silica in grain #220. Blue: Spectrum displaying mainly the strongest peaks at 461 $cm^{-1}$; red: more detailed spectrum showing additional peaks and one pronounced at 1524 $cm^{-1}$.

**FIGURE 5.** Ternary plot of the CAS analyses, in wt%, highlighting the presence of eight different compositions. In the background, the liquidus surface of $SiO_2$-CaO-$Al_2O_3$ system at ambient pressure (Osborne and Muan 1960) is shown. The arrows indicate the direction of downward temperature gradient. In the cement chemistry jargon, "C" stands for CaO, "A" for $Al_2O_3$ and "S" for $SiO_2$ (example: $CAS_2$ = CaO + $Al_2O_3$ + $2SiO_2$ = $CaAl_2Si_2O_8$ = anorthite).

**TABLE 1.** Microprobe analyses of CAS phases.

bd : below detection ; na : not analyzed.

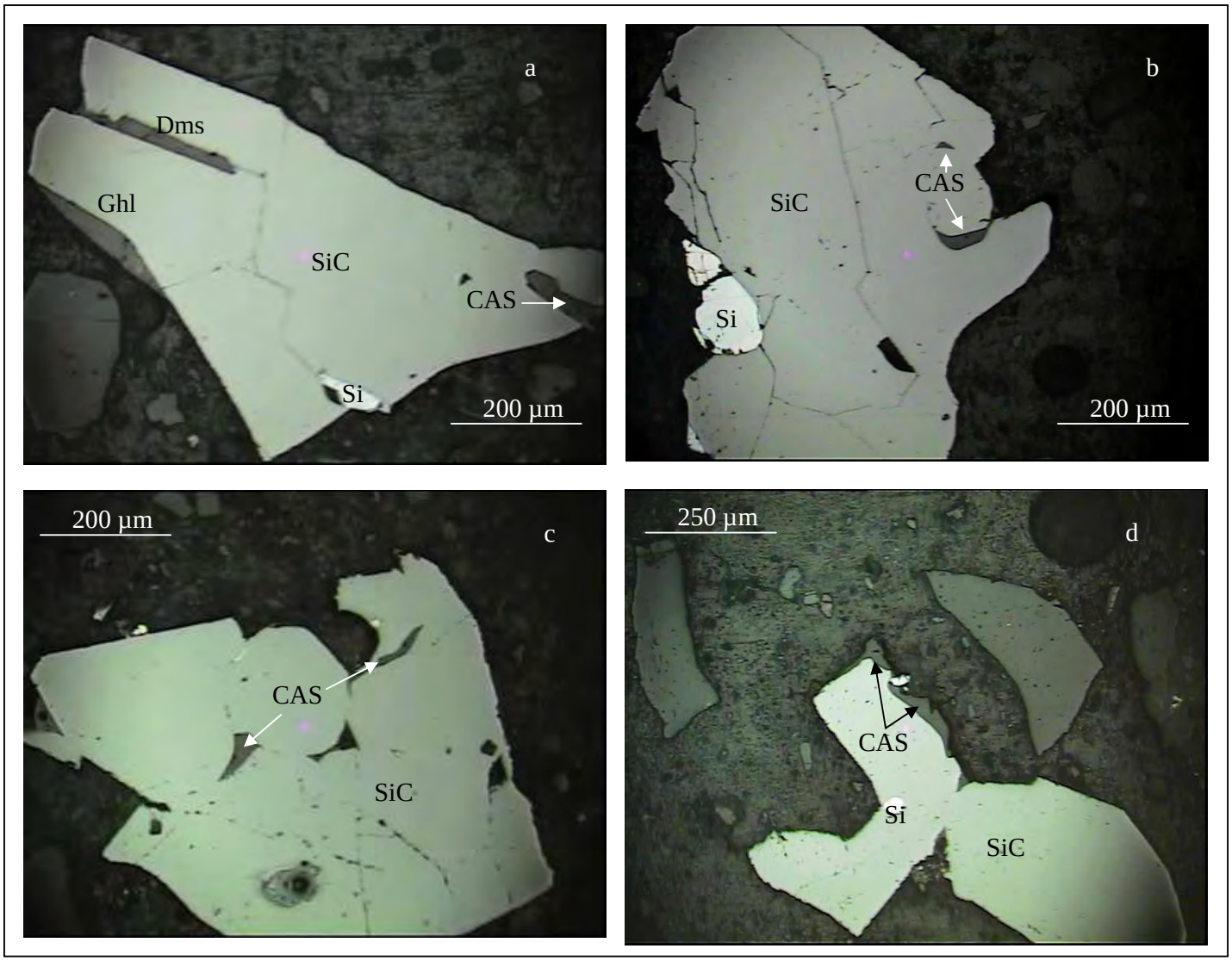


**FIGURE 1.** Thin section photos (reflected light) of Ca-Al-silicates (CAS) in contact or forming inclusions in moissanite crystals. (a) SiC #78: system of multiple inclusions. CAS are in grey, metallic Si in white. The grey crystal growing on the left rim is gehlenite (Ghl: analyses 21-24 in Table 1). The crystal above is Dmisteinbergite (Dms: analysis 17 in Table 1). The CAS crystal to the right has $Ca_{1-x}(Al,Si)_{3+x}O_6$ composition. (b) SiC #199: the two grey inclusions of CAS are arrowed. Details of the larger CAS inclusion, along with the EDS X-ray mapping, are presented in figure 2. (c) SiC #85 containing two grey inclusions of CAS. (d) SiC #244 with a CAS crystal (arrowed: analyses 2-4, and 10-11 in Table 1) on the surface, and

associated with a TiN grain, in white. Details of this grain, along with the EDS X-ray mapping, are presented in figure 3

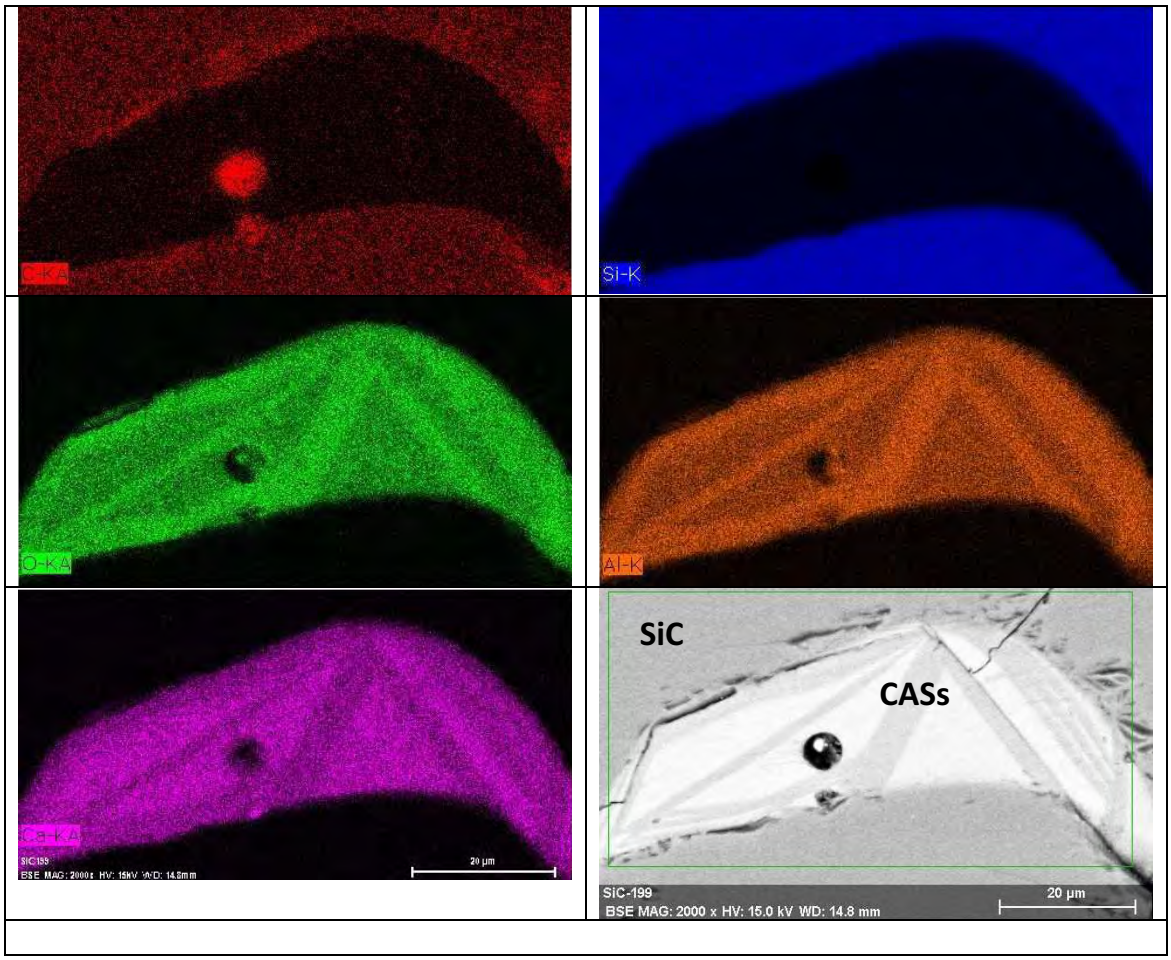


**FIGURE 2.** X-Ray mapping of CAS inclusion in SiC #199. Dark lamellae in the BSE image are dmisteinbergite, while bright areas have a $Ca_x(Al,Si)_{1-x}O_3$ composition.

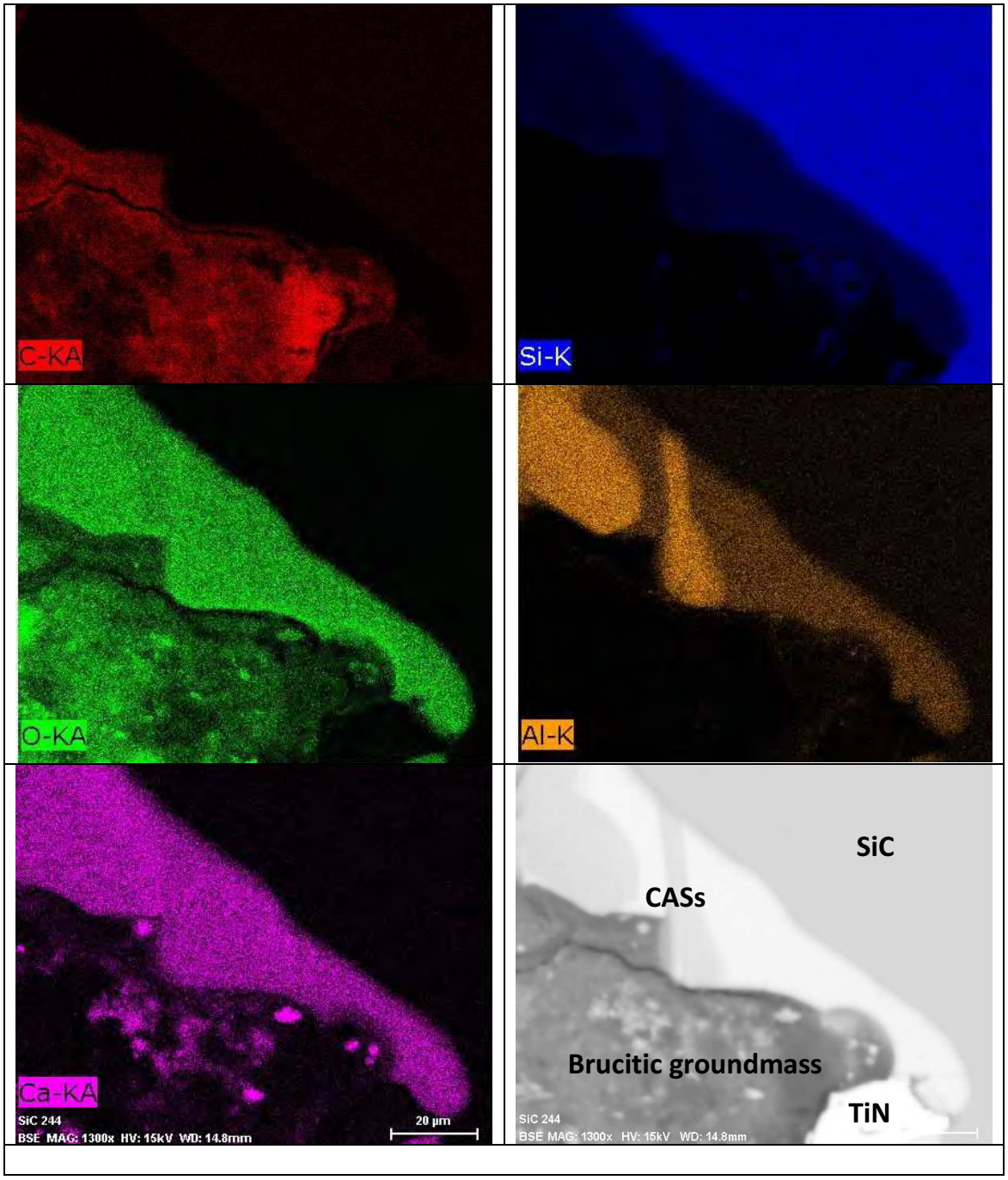


**FIGURE 3.** X-Ray mapping of CAS inclusion in SiC #244. Dark lamellae in BSE image are Dmisteinbergite (Table 1, analyses 10 and 11), while bright areas have a $Ca_{1-x}(Al,Si)_{2+x}O_5$ composition (Table 1, analyses 2 to 4).

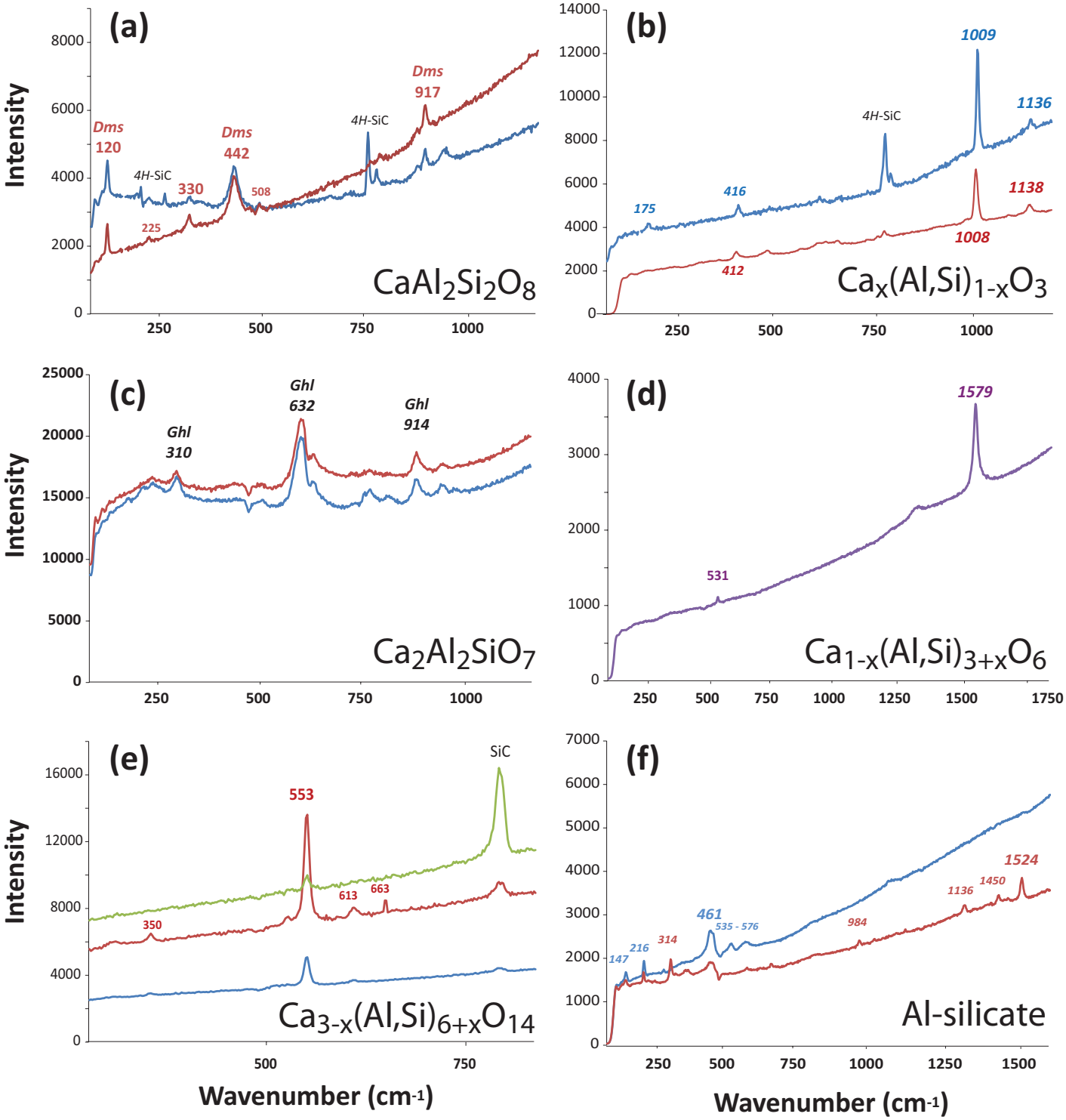
(a)
Intensity
Dms 120
4H-SiC
330
225
Dms 442
508
4H-SiC
Dms 917
CaAl2Si2O8
(b)
1009
1136
4H-SiC
175
416
1138
1008
412
Cax(Al,Si)1-xO3
(c)
Ghl 310
Ghl 632
Ghl 914
Ca2Al2SiO7
(d)
1579
531
Ca1-x(Al,Si)3+xO6
(e)
SiC
553
613
663
350
Ca3-x(Al,Si)6+xO14
(f)
1524
1450
1136
461
535 - 576
984
314
216
147
Al-silicate
Wavenumber (cm-1)
Wavenumber (cm-1)

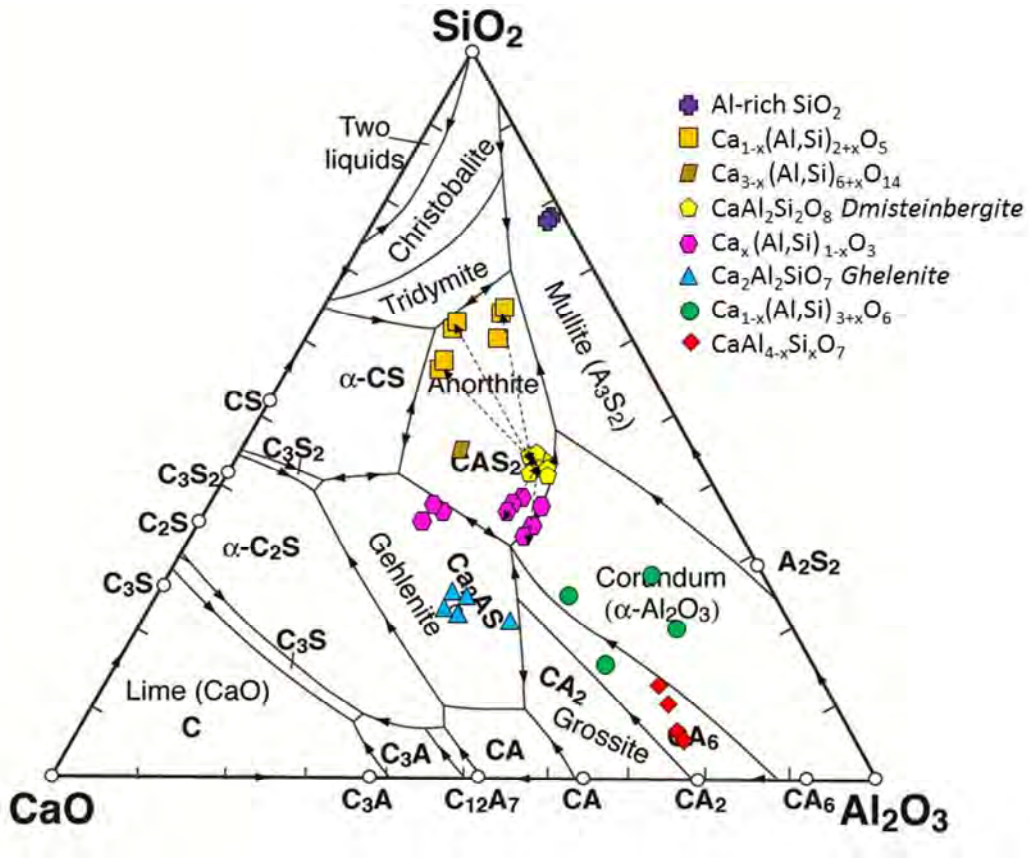


**FIGURE 5.** $SiO_2$-CaO-$Al_2O_3$ ternary plot of all the EMPA analyses, in wt%, highlighting the presence of eight different compositions. In the background, the CAS system at ambient pressure (Osborne and Muan 1960). In the cement chemistry jargon, "C" stands for CaO, "A" for $Al_2O_3$ and "S" for $SiO_2$ (example: $CAS_2$ = CaO + $Al_2O_3$ + $2SiO_2$ = $CaAl_2Si_2O_8$ = anorthite).

**Table 1.** Microprobe analyses of CAS phases

| # hosting SiC | 13 | 78 | 273 | | 29 | 29 | | 78 | 78 | 78 | 250 | 250 | 250 | 250 | 49 | 49 |
|---|---|---|---|---|---|---|---|---|---|---|---|---|---|---|---|---|
| # µ-probe | #1 | #18 | #46 | | #59 | #60 | | #10 | #11 | #12 | #33 | #35 | #36 | #38 | #62 | #63 |
| | $Ca_{1-x}(Al,Si)_{3+x}O_6$ | | | | $CaAl_{4-x}Si_xO_7$ | | | $Ca_x(Al,Si)_{1-x}O_3$ | | | | | | | | |
| $SiO_2$ | 18.01 | 20.87 | 28.16 | | 5.66 | 4.72 | | 37.77 | 34.37 | 32.59 | 37.08 | 37.99 | 37.21 | 37.56 | 36.92 | 36.25 |
| $TiO_2$ | bd | bd | bd | | bd | bd | | bd | bd | bd | bd | bd | bd | bd | bd | bd |
| $ZrO_2$ | bd | bd | bd | | bd | bd | | bd | bd | bd | bd | bd | bd | bd | bd | bd |
| $Al_2O_3$ | 58.73 | 64.01 | 56.86 | | 75.06 | 76.15 | | 39.02 | 39.62 | 40.18 | 35.22 | 35.52 | 35.29 | 35.01 | 26.11 | 28.29 |
| $Y_2O_3$ | 0.14 | bd | bd | | bd | bd | | bd | bd | bd | bd | bd | 0.07 | 0.07 | bd | bd |
| $La_2O_3$ | bd | bd | bd | | bd | bd | | bd | 0.08 | bd | bd | bd | bd | 0.13 | bd | bd |
| $Ce_2O_3$ | bd | bd | bd | | 0.09 | bd | | bd | bd | bd | bd | bd | bd | 0.13 | bd | bd |
| FeO | bd | bd | 0.09 | | bd | bd | | 0.15 | bd | bd | bd | bd | bd | bd | bd | bd |
| MnO | bd | bd | bd | | bd | bd | | bd | bd | 0.08 | bd | bd | bd | bd | bd | bd |
| MgO | 0.11 | 0.22 | bd | | bd | bd | | 0.13 | 0.08 | 0.07 | 0.14 | 0.05 | 0.04 | 0.09 | 0.16 | 0.23 |
| CaO | 25.02 | 15.10 | 13.49 | | 21.24 | 21.51 | | 22.52 | 25.61 | 27.09 | 27.16 | 26.74 | 24.22 | 25.91 | 36.27 | 35.31 |
| SrO | 0.07 | bd | 0.08 | | 0.16 | 0.22 | | 0.12 | 0.08 | bd | bd | 0.11 | bd | 0.09 | 0.40 | 0.45 |
| BaO | 0.21 | 0.14 | 0.33 | | 0.22 | 0.06 | | 0.62 | 1.07 | 0.93 | 1.04 | 0.59 | 1.25 | 1.05 | 0.82 | 0.23 |
| $Na_2O$ | bd | bd | 0.09 | | bd | bd | | 0.08 | 0.11 | 0.14 | 0.04 | 0.05 | 0.04 | 0.07 | 0.33 | 0.34 |
| $K_2O$ | bd | 0.03 | 0.06 | | bd | bd | | 0.06 | 0.12 | 0.14 | 0.03 | bd | bd | 0.06 | 0.03 | bd |
| $SO_2$ | 0.37 | 0.17 | 0.47 | | 0.14 | bd | | 0.34 | 0.57 | 0.62 | 0.34 | 0.79 | 0.98 | 0.37 | 0.16 | bd |
| | | | | | | | | | | | | | | | | |
| Total | 102.66 | 100.54 | 99.65 | | 102.57 | 102.66 | | 100.81 | 101.71 | 101.84 | 101.05 | 101.84 | 99.10 | 100.54 | 101.20 | 101.10 |
| | | | | | | | | | | | | | | | | |
| Si | 0.65 | 0.73 | 0.99 | | 0.24 | 0.20 | | 0.67 | 0.62 | 0.59 | 0.67 | 0.68 | 0.69 | 0.68 | 0.69 | 0.68 |
| Ti | 0.00 | 0.00 | 0.00 | | 0.00 | 0.00 | | 0.00 | 0.00 | 0.00 | 0.00 | 0.00 | 0.00 | 0.00 | 0.00 | 0.00 |
| Zr | 0.00 | 0.00 | 0.00 | | 0.00 | 0.00 | | 0.00 | 0.00 | 0.00 | 0.00 | 0.00 | 0.00 | 0.00 | 0.00 | 0.00 |
| Al | 2.49 | 2.64 | 2.34 | | 3.71 | 3.76 | | 0.82 | 0.84 | 0.86 | 0.75 | 0.75 | 0.77 | 0.75 | 0.58 | 0.62 |
| Y | 0.00 | 0.00 | 0.00 | | 0.00 | 0.00 | | 0.00 | 0.00 | 0.00 | 0.00 | 0.00 | 0.00 | 0.00 | 0.00 | 0.00 |
| La | 0.00 | 0.00 | 0.00 | | 0.00 | 0.00 | | 0.00 | 0.00 | 0.00 | 0.00 | 0.00 | 0.00 | 0.00 | 0.00 | 0.00 |
| Ce | 0.00 | 0.00 | 0.00 | | 0.00 | 0.00 | | 0.00 | 0.00 | 0.00 | 0.00 | 0.00 | 0.00 | 0.00 | 0.00 | 0.00 |
| Fe | 0.00 | 0.00 | 0.00 | | 0.00 | 0.00 | | 0.00 | 0.00 | 0.00 | 0.00 | 0.00 | 0.00 | 0.00 | 0.00 | 0.00 |
| Mn | 0.00 | 0.00 | 0.00 | | 0.00 | 0.00 | | 0.00 | 0.00 | 0.00 | 0.00 | 0.00 | 0.00 | 0.00 | 0.00 | 0.00 |
| Mg | 0.01 | 0.01 | 0.00 | | 0.00 | 0.00 | | 0.00 | 0.00 | 0.00 | 0.00 | 0.00 | 0.00 | 0.00 | 0.00 | 0.01 |
| Ca | 0.96 | 0.57 | 0.51 | | 0.96 | 0.97 | | 0.43 | 0.49 | 0.53 | 0.53 | 0.51 | 0.48 | 0.50 | 0.73 | 0.70 |
| Sr | 0.00 | 0.00 | 0.00 | | 0.00 | 0.01 | | 0.00 | 0.00 | 0.00 | 0.00 | 0.00 | 0.00 | 0.00 | 0.00 | 0.00 |
| Ba | 0.00 | 0.00 | 0.00 | | 0.00 | 0.00 | | 0.00 | 0.01 | 0.01 | 0.01 | 0.00 | 0.01 | 0.01 | 0.01 | 0.00 |
| Na | 0.00 | 0.00 | 0.01 | | 0.00 | 0.00 | | 0.00 | 0.00 | 0.00 | 0.00 | 0.00 | 0.00 | 0.00 | 0.01 | 0.01 |
| K | 0.00 | 0.00 | 0.00 | | 0.00 | 0.00 | | 0.00 | 0.00 | 0.00 | 0.00 | 0.00 | 0.00 | 0.00 | 0.00 | 0.00 |
| S | 0.01 | 0.01 | 0.02 | | 0.01 | 0.00 | | 0.01 | 0.01 | 0.01 | 0.01 | 0.01 | bd | 0.01 | 0.00 | 0.00 |
| | | | | | | | | | | | | | | | | |
| ∑ cations | 4.13 | 3.96 | 3.87 | | 4.92 | 4.93 | | 1.94 | 1.98 | 2.00 | 1.97 | 1.96 | 1.96 | 1.96 | 2.04 | 2.03 |
| | | | | | | | | | | | | | | | | |
| N. Oxygen | 6 | 6 | 6 | | 7 | 7 | | 3 | 3 | 3 | 3 | 3 | 3 | 3 | 3 | 3 |

Table 1 – microprobe analyses of CAS Revision 1

| # hosting SiC | 78 | 78 | 78 | 78 | 78 | 78 | | 78 | 250 | 272 | 273 | 273 | 175 | 175 | 175 | 175 | 175 | 244 | 244 |
|---|---|---|---|---|---|---|---|---|---|---|---|---|---|---|---|---|---|---|---|
| # µ-probe | #5 | #8 | #21 | #22 | #23 | #24 | | #17 | #37 | #39 | #44 | #45 | #51 | #52 | #54 | #55 | #56 | #10 | #11 |
| | **$Ca_2Al_2SiO_7$ - *Ghelenite*** | | | | | | | **$CaAl_2Si_2O_8$ - *Dmisteinbergite*** | | | | | | | | | | | |
| $SiO_2$ | 23.48 | 22.62 | 25.43 | 21.98 | 24.73 | 25.06 | | 40.41 | 40.37 | 40.52 | 44.53 | 43.87 | 40.69 | 42.48 | 44.06 | 41.61 | 43.83 | 44.06 | 40.59 |
| $TiO_2$ | bd | bd | bd | bd | bd | bd | | bd | bd | bd | 0.06 | 0.08 | bd | bd | bd | bd | bd | bd | bd |
| $ZrO_2$ | bd | bd | bd | bd | bd | bd | | bd | bd | bd | bd | bd | bd | bd | bd | bd | bd | bd | bd |
| $Al_2O_3$ | 37.01 | 38.44 | 36.84 | 45.17 | 38.61 | 39.10 | | 38.37 | 36.92 | 36.01 | 35.54 | 34.16 | 36.16 | 36.17 | 34.93 | 37.49 | 36.53 | 36.12 | 38.57 |
| $Y_2O_3$ | bd | bd | bd | bd | bd | bd | | bd | bd | bd | bd | bd | bd | bd | bd | bd | bd | bd | bd |
| $La_2O_3$ | bd | 0.09 | bd | bd | bd | bd | | bd | bd | bd | bd | bd | bd | bd | bd | bd | bd | 0.10 | 0.09 |
| $Ce_2O_3$ | bd | bd | bd | bd | bd | bd | | bd | bd | bd | bd | bd | bd | bd | 0.14 | bd | bd | 0.19 | bd |
| FeO | bd | bd | bd | bd | bd | bd | | bd | bd | bd | 0.39 | 0.29 | bd | bd | 0.27 | 0.13 | 0.11 | bd | 0.08 |
| MnO | bd | bd | bd | bd | bd | bd | | bd | bd | bd | bd | bd | bd | bd | 0.03 | 0.02 | bd | bd | bd |
| MgO | bd | bd | bd | bd | bd | bd | | 0.11 | bd | 0.06 | bd | 0.75 | 0.09 | bd | 0.08 | 0.05 | bd | bd | 0.05 |
| CaO | 40.09 | 38.21 | 38.10 | 32.91 | 36.38 | 36.49 | | 20.20 | 20.43 | 21.94 | 18.07 | 18.16 | 20.89 | 19.47 | 19.85 | 20.63 | 19.62 | 19.67 | 19.52 |
| SrO | bd | 0.17 | 0.09 | 0.10 | bd | 0.08 | | 0.08 | 0.09 | 0.09 | 0.15 | 0.08 | 0.06 | 0.12 | bd | 0.08 | bd | bd | bd |
| BaO | bd | 0.32 | 0.18 | 0.33 | 0.33 | 0.16 | | 0.79 | 1.33 | 1.33 | 0.54 | 0.58 | 0.99 | 0.79 | 1.75 | 1.07 | 0.82 | 0.44 | 0.49 |
| $Na_2O$ | bd | bd | 0.06 | 0.04 | bd | bd | | bd | bd | 0.05 | 0.19 | 0.16 | 0.04 | bd | bd | 0.04 | bd | 0.08 | 0.09 |
| $K_2O$ | bd | bd | bd | bd | bd | bd | | 0.07 | bd | 0.05 | 0.12 | 0.11 | 0.03 | bd | 0.03 | 0.03 | bd | 0.05 | 0.07 |
| $SO_2$ | 0.07 | 0.19 | 0.21 | 0.51 | 0.18 | 0.11 | | 0.13 | 0.19 | 0.10 | 1.76 | 1.20 | 0.69 | bd | 0.21 | 0.25 | bd | 0.03 | bd |
| | | | | | | | | | | | | | | | | | | | |
| Total | 100.65 | 100.04 | 100.91 | 101.04 | 100.23 | 101.00 | | 100.16 | 99.33 | 100.15 | 101.35 | 99.44 | 99.64 | 99.03 | 101.35 | 101.40 | 100.91 | 100.74 | 99.55 |
| | | | | | | | | | | | | | | | | | | | |
| Si | 1.06 | 1.03 | 1.13 | 0.97 | 1.10 | 1.11 | | 1.90 | 1.92 | 1.92 | 2.07 | 2.07 | 1.94 | 2.00 | 2.05 | 1.94 | 2.02 | 2.03 | 1.90 |
| Ti | 0.00 | 0.00 | 0.00 | 0.00 | 0.00 | 0.00 | | 0.00 | 0.00 | 0.00 | 0.00 | 0.00 | 0.00 | 0.00 | 0.00 | 0.00 | 0.00 | 0.00 | 0.00 |
| Zr | 0.00 | 0.00 | 0.00 | 0.00 | 0.00 | 0.00 | | 0.00 | 0.00 | 0.00 | 0.00 | 0.00 | 0.00 | 0.00 | 0.00 | 0.00 | 0.00 | 0.00 | 0.00 |
| Al | 1.96 | 2.06 | 1.94 | 2.34 | 2.03 | 2.04 | | 2.12 | 2.07 | 2.02 | 1.95 | 1.90 | 2.03 | 2.01 | 1.92 | 2.06 | 1.99 | 1.97 | 2.13 |
| Y | 0.00 | 0.00 | 0.00 | 0.00 | 0.00 | 0.00 | | 0.00 | 0.00 | 0.00 | 0.00 | 0.00 | 0.00 | 0.00 | 0.00 | 0.00 | 0.00 | 0.00 | 0.00 |
| La | 0.00 | 0.00 | 0.00 | 0.00 | 0.00 | 0.00 | | 0.00 | 0.00 | 0.00 | 0.00 | 0.00 | 0.00 | 0.00 | 0.00 | 0.00 | 0.00 | 0.00 | 0.00 |
| Ce | 0.00 | 0.00 | 0.00 | 0.00 | 0.00 | 0.00 | | 0.00 | 0.00 | 0.00 | 0.00 | 0.00 | 0.00 | 0.00 | 0.00 | 0.00 | 0.00 | 0.00 | 0.00 |
| Fe | 0.00 | 0.00 | 0.00 | 0.00 | 0.00 | 0.00 | | 0.00 | 0.00 | 0.00 | 0.02 | 0.01 | 0.00 | 0.00 | 0.01 | 0.00 | 0.00 | 0.00 | 0.00 |
| Mn | 0.00 | 0.00 | 0.00 | 0.00 | 0.00 | 0.00 | | 0.00 | 0.00 | 0.00 | 0.00 | 0.00 | 0.00 | 0.00 | 0.00 | 0.00 | 0.00 | 0.00 | 0.00 |
| Mg | 0.00 | 0.00 | 0.00 | 0.00 | 0.00 | 0.00 | | 0.01 | 0.00 | 0.00 | 0.00 | 0.05 | 0.01 | 0.00 | 0.01 | 0.00 | 0.00 | 0.00 | 0.00 |
| Ca | 1.93 | 1.86 | 1.82 | 1.55 | 1.74 | 1.73 | | 1.02 | 1.04 | 1.12 | 0.90 | 0.92 | 1.07 | 0.98 | 0.99 | 1.03 | 0.97 | 0.97 | 0.98 |
| Sr | 0.00 | 0.00 | 0.00 | 0.00 | 0.00 | 0.00 | | 0.00 | 0.00 | 0.00 | 0.00 | 0.00 | 0.00 | 0.00 | 0.00 | 0.00 | 0.00 | 0.00 | 0.00 |
| Ba | 0.00 | 0.01 | 0.00 | 0.01 | 0.01 | 0.00 | | 0.01 | 0.02 | 0.02 | 0.01 | 0.01 | 0.02 | 0.01 | 0.03 | 0.02 | 0.01 | 0.01 | 0.01 |
| Na | 0.00 | 0.00 | 0.00 | 0.00 | 0.00 | 0.00 | | 0.00 | 0.00 | 0.00 | 0.02 | 0.01 | 0.00 | 0.00 | 0.00 | 0.00 | 0.00 | 0.01 | 0.01 |
| K | 0.00 | 0.00 | 0.00 | 0.00 | 0.00 | 0.00 | | 0.00 | 0.00 | 0.00 | 0.01 | 0.01 | 0.00 | 0.00 | 0.00 | 0.00 | 0.00 | 0.00 | 0.00 |
| S | 0.00 | 0.01 | 0.00 | 0.01 | 0.01 | 0.00 | | 0.01 | 0.01 | 0.00 | 0.08 | 0.05 | 0.03 | 0.00 | 0.01 | 0.01 | 0.00 | 0.00 | 0.00 |
| | | | | | | | | | | | | | | | | | | | |
| ∑ cations | 4.97 | 4.96 | 4.90 | 4.87 | 4.89 | 4.88 | | 5.07 | 5.08 | 5.10 | 5.06 | 5.05 | 5.10 | 5.01 | 5.03 | 5.07 | 5.00 | 5.00 | 5.05 |
| | | | | | | | | | | | | | | | | | | | |
| N. Oxygen | 7 | 7 | 7 | 7 | 7 | 7 | | 8 | 8 | 8 | 8 | 8 | 8 | 8 | 8 | 8 | 8 | 8 | 8 |

Table 1 – microprobe analyses of CAS Revision 1

| # hosting SiC | 244 | 244 | 244 | 272 | 272 | 272 | | 220 | 220 | | | 49 | |
|---|---|---|---|---|---|---|---|---|---|---|---|---|---|
| # µ-probe | #2 | #3 | #4 | #40 | #41 | #42 | | #13 | #14 | | | #65 | |
| | **$Ca_{1-x}(Al.Si)_{2+x}O_5$** | | | | | | | **Al-bearing $SiO_2$** | | | | **$Ca_{3-x}(Al.Si)_{6+x}O_{14}$** | |
| $SiO_2$ | 56.75 | 49.40 | 51.59 | 61.88 | 59.03 | 62.31 | | 65.39 | 66.39 | | | 43.04 | |
| $TiO_2$ | bd | bd | bd | bd | bd | bd | | bd | bd | | | bd | |
| $ZrO_2$ | 0.21 | 0.34 | 0.34 | bd | bd | bd | | 0.90 | 0.86 | | | bd | |
| $Al_2O_3$ | 15.45 | 14.97 | 14.85 | 20.10 | 21.84 | 20.01 | | 17.65 | 17.22 | | | 25.38 | |
| $Y_2O_3$ | 0.52 | 1.05 | 0.98 | bd | 0.11 | bd | | bd | bd | | | bd | |
| $La_2O_3$ | 0.14 | 0.18 | 0.36 | bd | bd | bd | | bd | bd | | | bd | |
| $Ce_2O_3$ | 0.36 | 0.76 | 0.72 | 0.08 | 0.09 | bd | | 0.37 | 0.44 | | | 0.11 | |
| FeO | bd | bd | bd | bd | bd | bd | | bd | bd | | | bd | |
| MnO | bd | 0.11 | 0.10 | bd | bd | bd | | bd | bd | | | bd | |
| MgO | 0.33 | 0.45 | 0.48 | 0.06 | 0.10 | 0.07 | | 0.14 | 0.17 | | | 0.43 | |
| CaO | 19.49 | 23.08 | 23.07 | 14.43 | 16.12 | 14.08 | | 1.67 | 1.70 | | | 27.37 | |
| SrO | bd | bd | bd | 0.07 | bd | bd | | bd | bd | | | 0.81 | |
| BaO | 2.94 | 2.77 | 2.94 | 1.24 | 1.19 | 1.19 | | 5.97 | 6.04 | | | 1.00 | |
| $Na_2O$ | bd | 0.09 | 0.12 | 0.20 | 0.19 | 0.20 | | 0.81 | 0.71 | | | 0.28 | |
| $K_2O$ | 0.46 | 0.28 | 0.24 | 0.20 | 0.17 | 0.20 | | 2.01 | 2.21 | | | 0.06 | |
| $SO_2$ | 0.88 | 1.59 | 1.55 | 1.72 | 1.61 | 1.60 | | 2.42 | 2.33 | | | 0.17 | |
| F | 1.60 | 3.91 | 3.80 | na | na | na | | na | na | | | na | |
| Cl | 0.04 | 0.05 | bd | na | na | na | | na | na | | | na | |
| Total | 99.17 | 99.03 | 101.14 | 99.98 | 100.45 | 99.66 | | 97.33 | 98.07 | | | 98.65 | |
| | | | | | | | | | | | | | |
| Si | 1.75 | 1.64 | 1.66 | 1.77 | 1.69 | 1.77 | | 3.15 | 3.17 | | | 3.74 | |
| Ti | 0.00 | 0.00 | 0.00 | 0.00 | 0.00 | 0.00 | | 0.00 | 0.00 | | | 0.00 | |
| Zr | 0.00 | 0.01 | 0.01 | 0.00 | 0.00 | 0.00 | | 0.02 | 0.02 | | | 0.00 | |
| Al | 0.56 | 0.58 | 0.56 | 0.68 | 0.74 | 0.67 | | 1.00 | 0.97 | | | 2.60 | |
| Y | 0.01 | 0.02 | 0.02 | 0.00 | 0.00 | 0.00 | | 0.00 | 0.00 | | | 0.00 | |
| La | 0.00 | 0.00 | 0.00 | 0.00 | 0.00 | 0.00 | | 0.00 | 0.00 | | | 0.00 | |
| Ce | 0.00 | 0.01 | 0.01 | 0.00 | 0.00 | 0.00 | | 0.01 | 0.01 | | | 0.00 | |
| Fe | 0.00 | 0.00 | 0.00 | 0.00 | 0.00 | 0.00 | | 0.00 | 0.00 | | | 0.00 | |
| Mn | 0.00 | 0.00 | 0.00 | 0.00 | 0.00 | 0.00 | | 0.00 | 0.00 | | | 0.00 | |
| Mg | 0.02 | 0.02 | 0.02 | 0.00 | 0.00 | 0.00 | | 0.01 | 0.01 | | | 0.06 | |
| Ca | 0.64 | 0.82 | 0.80 | 0.44 | 0.50 | 0.43 | | 0.09 | 0.09 | | | 2.55 | |
| Sr | 0.00 | 0.00 | 0.00 | 0.00 | 0.00 | 0.00 | | 0.00 | 0.00 | | | 0.04 | |
| Ba | 0.04 | 0.04 | 0.04 | 0.01 | 0.01 | 0.01 | | 0.11 | 0.11 | | | 0.03 | |
| Na | 0.00 | 0.01 | 0.01 | 0.01 | 0.01 | 0.01 | | 0.08 | 0.07 | | | 0.05 | |
| K | 0.02 | 0.01 | 0.01 | 0.01 | 0.01 | 0.01 | | 0.12 | 0.13 | | | 0.01 | |
| S | 0.03 | 0.05 | 0.05 | 0.05 | 0.04 | 0.04 | | 0.11 | 0.10 | | | 0.01 | |
| | | | | | | | | | | | | | |
| ∑ cations | 3.06 | 3.20 | 3.18 | 2.97 | 2.95 | 2.95 | | 4.70 | 4.69 | | | 9.09 | |
| | | | | | | | | | | | | | |
| N. Oxygen | 5 | 5 | 5 | 5 | 5 | 5 | | 8 | 8 | | | 14 | |

bd : below detection ; na : not analyzed